

# High-precision measurements of the atomic mass and electron-capture decay $Q$ value of $^{95}\text{Tc}$

Zhuang Ge<sup>a,\*</sup>, Tommi Eronen<sup>a</sup>, Vasile Alin Sevestrean<sup>b,c,d,\*</sup>, Ovidiu Nițescu<sup>b,d</sup>, Sabin Stoica<sup>b</sup>, Marlon Ramalho<sup>a</sup>, Jouni Suhonen<sup>a,b,\*</sup>, Antoine de Roubin<sup>e,f</sup>, Dmitrii Nesterenko<sup>a</sup>, Anu Kankainen<sup>a</sup>, Pauline Ascher<sup>f</sup>, Samuel Ayet San Andres<sup>g</sup>, Olga Beliuskina<sup>a</sup>, Pierre Delahaye<sup>h</sup>, Mathieu Flayol<sup>f</sup>, Mathias Gerbaux<sup>f</sup>, Stéphane Grévy<sup>f</sup>, Marjut Hukkanen<sup>a,i</sup>, Arthur Jaries<sup>a</sup>, Ari Jokinen<sup>a</sup>, Audric Husson<sup>f</sup>, Daid Kahl<sup>j,2</sup>, Joel Kostensalo<sup>k</sup>, Jenni Kotila<sup>b,l,m</sup>, Iain Moore<sup>a</sup>, Stylianos Nikas<sup>a</sup>, Marek Stryjczyk<sup>a</sup> and Ville Virtanen<sup>a</sup>

<sup>a</sup>Department of Physics, University of Jyväskylä, P.O. Box 35, FI-40014, Jyväskylä, Finland

<sup>b</sup>International Centre for Advanced Training and Research in Physics (CIFRA), POB MG-12, RO-077125, Bucharest-Măgurele, Romania

<sup>c</sup>Faculty of Physics, University of Bucharest, 405 Atomiștilor, POB MG-11, RO-077125, Bucharest-Măgurele, Romania

<sup>d</sup>Horia Hulubei" National Institute of Physics and Nuclear Engineering, 30 Reactorului, POB MG-6, RO-077125, Bucharest-Măgurele, Romania

<sup>e</sup>KU Leuven, Instituut voor Kern- en Stralingsfysica, B-3001, Leuven, Belgium

<sup>f</sup>Université de Bordeaux, CNRS/IN2P3, UMR 5797, F-33170, Gradignan, France

<sup>g</sup>Instituto de Física Corpuscular, CSIC-UV, 46980, Gradignan, Spain

<sup>h</sup>GANIL, CEA/DSM-CNRS/IN2P3, Bd Henri Becquerel, 14000, Caen, France

<sup>i</sup>Université de Bordeaux, CNRS/IN2P3, LP2I Bordeaux, UMR 5797, F-33170, Gradignan, France

<sup>j</sup>Extreme Light Infrastructure - Nuclear Physics, Horia Hulubei National Institute for R&D in Physics and Nuclear Engineering (IFIN-HH), 077125, Bucharest-Măgurele, Romania

<sup>k</sup>Natural Resources Institute Finland, Yliopistonkatu 6B, FI-80100, Joensuu, Finland

<sup>l</sup>Finnish Institute for Educational Research, University of Jyväskylä, P.O. Box 35, FI-40014, Jyväskylä, Finland

<sup>m</sup>Center for Theoretical Physics, Sloane Physics Laboratory, Yale University, New Haven, Connecticut 06520-8120, Connecticut, USA

## ARTICLE INFO

### Keywords:

Penning trap  
mass measurements  
ultra-low  $Q$  value  
electron capture  
neutrino mass

## ABSTRACT

A direct measurement of the ground-state-to-ground-state electron-capture decay  $Q$  value of  $^{95}\text{Tc}$  has been performed utilizing the double Penning trap mass spectrometer JYFLTRAP. The  $Q$  value was determined to be 1695.92(13) keV by taking advantage of the high resolving power of the phase-imaging ion-cyclotron-resonance technique to resolve the low-lying isomeric state of  $^{95}\text{Tc}$  (excitation energy of 38.910(40) keV) from the ground state. The mass excess of  $^{95}\text{Tc}$  was measured to be  $-86015.95(18)$  keV/c<sup>2</sup>, exhibiting a precision of about 28 times higher and in agreement with the value from the newest Atomic Mass Evaluation (AME2020). Combined with the nuclear energy-level data for the decay-daughter  $^{95}\text{Mo}$ , two potential ultra-low  $Q$ -value transitions are identified for future long-term neutrino-mass determination experiments. The atomic self-consistent many-electron Dirac–Hartree–Fock–Slater method and the nuclear shell model have been used to predict the partial half-lives and energy-release distributions for the two transitions. The dominant correction terms related to those processes are considered, including the exchange and overlap corrections, and the shake-up and shake-off effects. The normalized distribution of the released energy in the electron-capture decay of  $^{95}\text{Tc}$  to excited states of  $^{95}\text{Mo}$  is compared to that of  $^{163}\text{Ho}$  currently being used for electron-neutrino-mass determination.

\*Principal corresponding authors

✉ zhuang.z.ge@jyu.fi (Zhuang Ge); sevestrean.alin@theory.nipne.ro (Vasile Alin Sevestrean); jouni.t.suhonen@jyu.fi (Jouni Suhonen)  
ORCID(s): 0000-0001-8586-6134 (Zhuang Ge); 0000-0003-0003-6022 (Tommi Eronen); 0009-0009-9658-2386 (Vasile Alin Sevestrean); 0000-0002-9598-8415 (Ovidiu Nițescu); 0000-0003-4632-7327 (Sabin Stoica); 0000-0003-3514-6678 (Marlon Ramalho); 0000-0002-9898-660X (Jouni Suhonen); 0000-0002-6103-2845 (Dmitrii Nesterenko); 0000-0003-1082-7602 (Anu Kankainen); 0000-0002-1990-0848 (Pauline Ascher); 0000-0002-0053-1691 (Samuel Ayet San Andres); 0000-0003-4448-7650 (Olga Beliuskina); 0000-0002-8851-7826 (Pierre Delahaye); 0000-0002-1215-2269 (Mathieu Flayol); 0000-0002-4317-3628 (Marjut Hukkanen); 0000-0002-5279-0820 (Arthur Jaries); 0000-0002-0451-125X (Ari Jokinen); 0000-0001-9798-0655 (Audric Husson); 0000-0003-3368-7307 (Daid Kahl); 0000-0001-9883-1256 (Joel Kostensalo); 0000-0001-9207-5824 (Jenni Kotila); 0000-0003-0934-8727 (Iain Moore); 0000-0001-6515-2409 (Marek Stryjczyk); 0000-0003-0276-6483 (Ville Virtanen)

<sup>1</sup>Present address: Facility for Rare Isotope Beams, Michigan State University, 640 South Shaw Lane East Lansing, MI 48824, USA

Neutrino oscillations in atmospheric, solar, and reactor neutrinos have confirmed that at least two neutrino mass eigenstates have non-zero rest mass. However, these oscillations cannot assess the absolute mass scale, but only the squared differences of the mass eigenstates [1, 2, 3]. Neutrinos are the second most abundant particles in the universe, and play an important role on cosmological scales [4]. Accurate measurements of the total neutrino mass involve their imprint on the cosmic microwave background (CMB) as well as on structure formation in the early universe.

The most direct method to measure the absolute mass scale of antineutrinos involves studying the electron energy spectrum of  $\beta^-$  decay. Though the neutrinoless double  $\beta^-$ -decay experiments can be used to infer the effective Majorana-neutrino mass from the measured lifetime, the exact relation depends on the mediator model and relies

on the calculation of the involved transition matrix elements [5, 6, 7, 8]. The ongoing leading experiment for the absolute neutrino mass scale determination is the Karlsruhe Tritium Neutrino (KATRIN)  $\beta^-$ -decay experiment which is designed to measure the electron-antineutrino mass,  $m_{\bar{\nu}_e}$ , with a sensitivity of  $0.2 \text{ eV}/c^2$  at 90% C.L. Most recently, KATRIN has set a limit of  $m_{\bar{\nu}_e} < 0.8 \text{ eV}/c^2$  (90% C.L.) [9, 10, 11]. Another experiment, Project 8, takes advantage of the cyclotron radiation emission spectroscopy (CRES) technique via measurements of the tritium end-point spectrum. The new technique CRES will allow for an eventual sensitivity to  $m_{\bar{\nu}_e}$  down to  $0.04 \text{ eV}/c^2$ . The first frequency-based neutrino mass limit of electron-weighted neutrino mass  $< 155 \text{ eV}/c^2$  is extracted from the background-free measurement of the continuous tritium  $\beta$  spectrum in a Bayesian (frequentist) analysis [12]. An alternative method in the ECHo [13, 14, 15, 16] and HOLMES [17, 18] experiments, uses electron capture (EC) on  $^{163}\text{Ho}$ , and has reached a current limit of  $150 \text{ eV}/c^2$  for the electron-neutrino mass [15].

A  $Q$  value as small as possible is desired in these single decay experiments for electron (anti)neutrino mass determination. The effective fraction of decays in a given energy interval  $\Delta E$  at the endpoint area will be larger with a lower  $Q$  value [19, 20]. Currently, only ground-state-to-ground-state (gs-to-gs) decay cases  $^3\text{H}$  ( $\beta$  decay) and  $^{163}\text{Ho}$  (electron capture), are being used for direct neutrino-mass-determination experiments. Ongoing intensive searches for isotopes undergoing  $\beta/\text{EC}$  decays from the ground state to an excited state with a low  $Q$  value are actively conducted at JYFLTRAP, LEBIT, CPT, ISOTRAP and SHIPTRAP Penning traps [21, 22, 23, 24, 25, 26, 27, 28, 29, 28, 30, 31, 32, 33, 34]. Penning trap mass spectrometry (PTMS) is the leading technique for accurate and precise mass and  $Q$  value determination, and it is hitherto the only direct method to measure the decay  $Q$  value to a sub-keV precision or better to verify whether a potential candidate is an ultra-low ( $< 1 \text{ keV}$ )  $Q$ -value transition or not.

In this article, we report on the first direct measurement of the gs-to-gs EC  $Q$  value of  $^{95}\text{Tc}$  with the JYFLTRAP PTMS. The precise  $Q$  value obtained in this study, in conjunction with nuclear energy level data for excited states of  $^{95}\text{Mo}$ , is utilized to ascertain their ground-state-to-excited-state (gs-to-es)  $Q$  values. In the case of  $^{95}\text{Tc}$ , there are two potential low  $Q$ -value gs-to-es EC transitions, that could be used for neutrino-mass detection. To explore this potential, we have utilized two computational approaches, the atomic self-consistent many-electron Dirac–Hartree–Fock–Slater method and the nuclear shell model, to predict the partial half-lives and energy-release distributions for the EC-decay transitions in question.

## 1. Experimental method

The experiment was performed at the Ion Guide Isotope Separator On-Line facility (IGISOL) using the JYFLTRAP

double Penning trap mass spectrometer [35] at the University of Jyväskylä, Finland [36, 37].

To generate  $^{95}\text{Tc}$  ions, a natural Mo target foil was irradiated with a few  $\mu\text{A}$  proton beam at 45 MeV from the K-130 cyclotron at the Accelerator Laboratory of the University of Jyväskylä. A helium-filled small volume gas cell was used to stop the recoils produced from the proton-induced fusion-evaporation reaction, and the ions were extracted using gas flow and guided through a sextupole ion guide [38] with a combination of DC and RF fields. Subsequently, the ions were accelerated with a 30 kV electric potential, followed by mass separation using a  $55^\circ$  dipole magnet with a typical mass resolving power of  $M/\Delta M \approx 500$ . After isobaric separation for ions of  $A/q = 95$ , including the reaction products  $^{95}\text{Nb}^+$ ,  $^{95m}\text{Tc}^+$ ,  $^{95}\text{Tc}^+$  and  $^{95}\text{Mo}^+$ , they were directed to a radiofrequency-quadrupole cooler-buncher (RFQ-CB) [39], where they underwent accumulation, cooling, and bunching.

Decay-daughter ions of  $^{95}\text{Mo}^+$  were prepared using the upstairs offline glow-discharge ion source. A  $90^\circ$  electrostatic bender selected ions either from the online target station or the offline ion source for downstream transmission.

JYFLTRAP comprises two cylindrical Penning traps in a 7-T superconducting solenoid. The first trap, functioning as a purification trap, is filled with helium buffer gas and is used for isobaric purification through the sideband buffer gas cooling technique [40]. This method achieves purification with a mass resolving power of  $\approx 10^5$ . In the purification trap, all cooled and centered ions ( $^{95}\text{Nb}^+$ ,  $^{95m}\text{Tc}^+$ ,  $^{95}\text{Tc}^+$ , and  $^{95}\text{Mo}^+$ ) are initially excited to a large magnetron motion orbit. This is accomplished by applying a dipole excitation at the magnetron motion frequency  $v_-$  for approximately 11 ms. Subsequently, a quadrupole excitation is executed for approximately 100 ms to center the ions of interest through collisions with the buffer gas. The buffer gas cooling technique eliminated  $^{95}\text{Mo}^+$  but did not have enough mass resolving power to remove the other aforementioned ions. To prepare mono-isotopic samples of  $^{95}\text{Tc}^+$ , the coupling of the dipolar excitation with Ramsey's method of time-separated oscillatory fields [41] and the phase-imaging ion-cyclotron-resonance (PI-ICR) technique [42, 43] was utilized, as described in details in [34]. A plot of the Ramsey-type dipole excitation frequency scan with a 5 ms (On) - 17 ms (Off) - 5 ms (On) excitation pattern in the second (precision) trap, filtered by the positional gates using the PI-ICR identification with a 755 ms phase accumulation time, is shown in Fig. 1.

For  $Q$ -value measurements, the PI-ICR method is used to measure the cyclotron frequency,  $v_c = qB/(2\pi m)$ , where  $B$  is the magnetic field strength,  $q$  is the charge and  $m$  the mass of the stored ion. The PI-ICR technique [43] provides around 40 times better resolving power than the conventional time-of-flight ion-cyclotron-resonance (TOF-ICR) method [43, 44, 45]. Two timing patterns are needed for the determination of  $v_c$ . The patterns differ only in their quadrupolar conversion pulse, separated in time by the defined phase-accumulation time,  $t_{acc}$ . The phase images of these two are projected onto a position-sensitive MCP

detector after the trap. Additionally a center point, measured without any excitations, is needed for angle determination.

The angle between two phase images of the projected radial motions with respect to the center spot is denoted as  $\alpha_c = \alpha_+ - \alpha_-$ , where  $\alpha_+$  and  $\alpha_-$  represent the polar angles of the cyclotron and magnetron motion phases. The cyclotron frequency  $v_c$  is derived from:  $v_c = (\alpha_c + 2\pi n_c)/2\pi t_{acc}$ , where  $n_c$  represents the full number of revolutions made by the measured ions during the phase accumulation time  $t_{acc}$ . Different accumulation times for  $^{95}\text{Tc}^+$  were utilized to unambiguously assign  $n_c$ . An accumulation time of 574 ms was employed for the actual measurements to determine the final  $v_c$  for both  $^{95}\text{Tc}^+$  and  $^{95}\text{Mo}^+$  ions; the choice also ensures that any leaked isobaric contaminant would not overlap with the ions of interest. The positions of the phase spots for magnetron and cyclotron motion were carefully selected to maintain an angle  $\alpha_c$  within a few degrees. This choice aimed to minimize the shift in the  $v_c$  ratio of the  $^{95}\text{Tc}^+$ - $^{95}\text{Mo}^+$  pair due to the conversion of the cyclotron motion to magnetron motion and the possible distortion of the ion-motion projection onto the detector to a level well below  $10^{-10}$  [44]. The excitation of the  $v_+$  delay was systematically scanned over one magnetron period, while the extraction delay varied over one cyclotron period. This accounted for any residual magnetron and cyclotron motion that might have shifted the different spots. The total data accumulation time of interleaved measurements of  $v_c$  for  $^{95}\text{Tc}^+$ - $^{95}\text{Mo}^+$  ions was  $\approx 4.9$  hours, respectively.

The gs-to-gs electron-capture  $Q$  value,  $Q_{\text{EC}}$ , can be derived from the mass difference of the decay pair:

$$Q_{\text{EC}} = (M_p - M_d)c^2 = (R-1)(M_d - qm_e)c^2 + (R \cdot B_d - B_p), \quad (1)$$

where  $M_p$  and  $M_d$  represent the masses of the parent and daughter atoms, respectively, and  $R (=v_{c,d}/v_{c,p})$  denotes their cyclotron frequency ratio for singly charged ions ( $q = 1$ ), with  $m_e$  being the mass of an electron. The electron binding energies of the parent and daughter atoms, denoted as  $B_p$  and  $B_d$ , are neglected due to their small values (on the order of a few eVs [46]), and  $R$  is close to 1. Since both the parent and daughter ions have the same  $A/q$  and their relative mass difference  $\Delta M/M < 10^{-4}$ , the mass-dependent error becomes negligible compared to the statistical uncertainty achieved in the measurements. Also, the contribution of uncertainty to the  $Q$  value from the mass uncertainty of the reference (daughter), which is 0.12 keV/c $^2$  for  $^{95}\text{Mo}$  [47], can be neglected.

## 2. Results and discussion

The determination of  $Q_{\text{EC}}$  depends on the measured cyclotron frequency ratio  $R$  via Eq. 1. Two data sets for  $^{95}\text{Tc}^+$ - $^{95}\text{Mo}^+$  were collected. A full scanning measurement of the magnetron phase, cyclotron phase and center spot in sequence (one cycle) was completed in less than 5 minutes for each ion species. In the analysis, the position of each spot was fit with the maximum likelihood method. A few

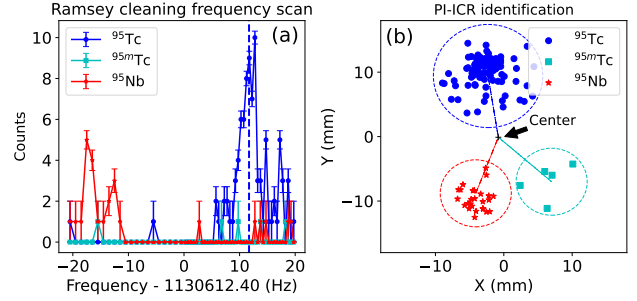


**Figure 1:** (Color online). (a) Ramsey-type dipole excitation frequency scan with a 5 ms (On) - 17 ms (Off) - 5 ms (On) excitation pattern in the second trap filtered by the positional gates shown in (b) using the PI-ICR identification (755 ms phase accumulation time) plot. The used angular gates are highlighted. The vertical dashed blue line shows the chosen optimal frequency to transmit  $^{95}\text{Tc}$  ions while suppressing the others.

cycles were summed to have reasonable statistics for fitting. The phase angles were calculated accordingly to deduce the cyclotron frequencies of each ion species. The cyclotron frequency  $v_c$  of the daughter  $^{95}\text{Mo}^+$  as a reference was linearly interpolated to the time of the measurement of the parent  $^{95}\text{Tc}^+$  (ion of interest) to deduce the cyclotron frequency ratio  $R$ . Only the bunches with less than five detected ions were considered in the data analysis in order to reduce a possible cyclotron frequency shift due to ion-ion interactions [52, 53]. The count-rate related frequency shifts were not observed in the analysis. The temporal fluctuation of the magnetic field  $\delta_B(v_c)/v_c = \Delta t \times 2.01(25) \times 10^{-12}/\text{min}$  [42], where  $\Delta t$  is the time interval between two consecutive reference measurements, is considered in the final results. Contribution of temporal fluctuations of the magnetic field to the final frequency ratio uncertainty was less than  $10^{-10}$  since the parent-daughter measurements were interleaved with  $\Delta t < 10$  minutes. The frequency shifts in the PI-ICR measurement due to ion image distortions were well below the statistical uncertainty and thus ignored in the calculation of the final uncertainty. Furthermore, decay pair ions  $^{95}\text{Tc}^+$ - $^{95}\text{Mo}^+$ , being mass doublets, cancel many of the systematic uncertainties in the cyclotron frequency ratio.

The weighted mean ratio  $\bar{R}$  of all single ratios was calculated along with the inner and outer errors to deduce the Birge ratio [54]. The maximum of the inner and outer errors was taken as the weight to calculate  $\bar{R}$ . In Fig. 2, results of the analysis including all data with comparison to literature values are demonstrated. The final parent-to-daughter frequency ratio  $\bar{R}$  with their uncertainty is determined to be 1.000 019 183 9(15). The corresponding gs-to-gs  $Q$  values is 1695.92(13) keV.

The gs-to-gs  $Q_{\text{EC}}$  value of 1695.92(13) keV from this work is  $\approx 37$  times more precise than that deduced from the evaluated masses in AME2020 [55, 47]. The measured  $Q_{\text{EC}}$  value has a deviation of 4.9(50) keV from the AME2020 value and is  $\approx 1\sigma$  larger. The  $Q_{\text{EC}}$  value in

**Table 1**

Potential candidate transitions of initial state (ground state) of parent nuclei  $^{95}\text{Tc}$  ( $9/2^+$ ) to the final states (excited states) of daughter  $^{95}\text{Mo}$  with ultra-low  $Q$  values. The first column lists the excited final state of  $^{95}\text{Mo}$  for the low  $Q$  value transition. The decay type is provided in the second column. The third and fourth columns present the derived decay  $Q_{\text{EC}}^*$  values in keV, sourced from literature (Lit.) [47] and this work (T. W.), respectively. The fifth column displays the experimental excitation energy  $E^*$  with its experimental error [48, 49, 50] in keV. The sixth column shows the confidence ( $\sigma$ ) of the  $Q_{\text{EC}}^*$  values being positive/negative. Columns seven to nine, denoted as  $\Delta_x$ , represent the distance of  $Q_{\text{EC}}^*$  values to the computed atomic relaxation energy following the electron capture  $\varepsilon_x$  in the daughter atoms [51]. FNU means forbidden non-unique. Spin-parity assignments and energy values enclosed in braces {} signify uncertain assignments or uncertainties in excitation energy, resulting in uncertainties in the decay type or decay energy. All the energies are in unit of keV.

Final state	Decay type	$Q_{\text{EC}}^*$ (Lit.)	$Q_{\text{EC}}^*$ (T. W.)	$E^*$	$Q/\delta Q$ (T. W.)	$\Delta_K$ (T. W.)	$\Delta_{L1}$ (T. W.)	$\Delta_{L2}$ (T. W.)
$^{95}\text{Mo}$ ( $9/2^+$ )	allowed	15.6(50)	20.52(61)	1675.40(60)	33	0.47(61)	17.64(61)	17.89(61)
$^{95}\text{Mo}$ ( $\{7/2^+, 9/2^+\}$ )	{allowed}	8.0(51)	12.9(10)	1683.0(10)	13		10.0(10)	10.3(10)
$^{95}\text{Mo}$ ( $1/2^+$ )	4th FNU	-1.0( $\{51\}$ )	3.92( $\{13\}$ )	1692({})	{29}		1.04( $\{13\}$ )	1.29( $\{13\}$ )

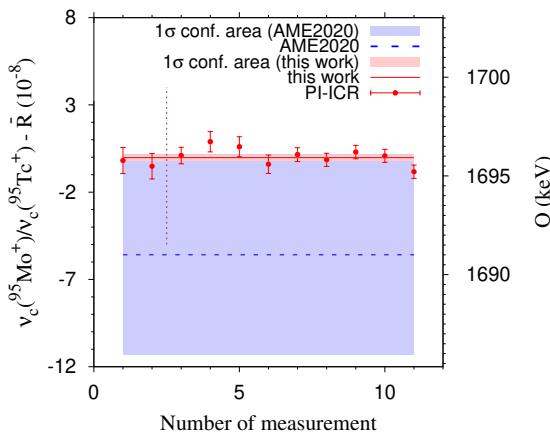


**Figure 2:** (Color online). The measured experimental results from this work compared to the literature values [55, 47]. The deviations of the individually measured cyclotron frequency ratios  $R$  ( $v_c(^{95}\text{Mo}^+)/v_c(^{95}\text{Tc}^+)$ ) from the measured value  $\bar{R}$  (left axis) and  $Q$  value (right axis) in this work are compared to values adopted from AME2020. The red points with uncertainties represent individual measurements using the PI-ICR method. Vertical brown dashed lines separate measurements conducted at different time slots. The weighted average value  $\bar{R}$  is depicted by the solid red line, and its  $1\sigma$  uncertainty band is shaded in red. The dashed blue line illustrates the difference between our new value and the one referenced in AME2020, with its  $1\sigma$  uncertainty area shaded in blue.

AME2020 is derived primarily from two  $\beta^+$ -decay experiments  $^{95}\text{Tc}(\beta^+)^{95}\text{Mo}$  [56, 57]. Combined with the atomic mass of  $^{95}\text{Mo}$  (mass excess:  $-87711.87(12)$  keV/c $^2$ ) from AME2020 [47, 55], we deduce the mass excess of its parent nucleus  $^{95}\text{Tc}$  ( $9/2^+$ ) to be  $-86015.95(18)$  keV/c $^2$ . The mass of  $^{95}\text{Tc}$  in AME2020 is primarily evaluated from  $\beta^+$ -decay experiments  $^{95}\text{Tc}(\beta^+)^{95}\text{Mo}$  and  $^{95}\text{Ru}(\beta^+)^{95}\text{Tc}$  with influence of 97.4% and 2.6%, respectively [56, 58, 59].

The high-precision electron-capture energy from this work, together with the nuclear energy level data from Ref. [48, 49, 50] of the excited states of  $^{95}\text{Mo}$  as tabulated in Table 1, was used to determine the gs-to-es  $Q$  value ( $Q_{\text{EC}}^*$ ) of three candidate states as shown in Table 1. The newly determined  $Q_{\text{EC}}^*$  confirm that the decay of the ground state

of  $^{95}\text{Tc}$  to the three excited states of interest are energetically allowed.

In case of EC, the closer the  $Q$  value of the decay to one of the ionization energies of the captured electrons, the larger the resonance enhancement of the rate near the endpoint, where the effects of a non-vanishing neutrino mass are relevant. The event-rate dependence on the  $Q$  value near the end-point for EC is steeper than that for  $\beta^-$  decay. As tabulated in Table 1,  $\Delta_x$  gives the distance of the  $Q_{\text{EC}}^*$  value to the computed atomic relaxation energy  $\varepsilon_x$  following the capture of electrons in the allowed daughter atomic shells ( $x = \text{K}, \text{L1}, \text{L2}$ , and other electrons from s-levels and p<sub>1/2</sub>-levels from the third and higher shells). For the state with the excitation energy of 1675.40(60) keV, the captures of electrons occupying the K and higher shells for the transition  $^{95}\text{Tc}$  ( $9/2^+$ )  $\rightarrow$   $^{95}\text{Mo}^*$  are energetically allowed, while for states with the excitation energy of 1683.0(10) keV and 1692 keV, only electrons from s-levels and p<sub>1/2</sub>-levels from the second (L) and higher shells can possibly be captured due to angular momentum conservation and the finite overlap of their wave function with the nucleus. The transition  $^{95}\text{Tc}$  ( $9/2^-$ )  $\rightarrow$   $^{95}\text{Mo}^*$  (1692 keV), giving the values of 1.04( $\{13\}$ ) keV and 1.29( $\{13\}$ ) keV for the distance of  $Q_{\text{EC}}^*$  to the computed atomic relaxation energy following the electron capture  $\varepsilon_{\text{L1}} = 2.878$  keV and  $\varepsilon_{\text{L2}} = 2.632$  keV, is of the decay type of 4<sup>th</sup> FNU (forbidden non-unique). It has a long half-life which will result in an extremely low fraction of events landing near the endpoint. This transition is not of interest for future neutrino mass determination due to the low branching ratio. To confirm whether the emitted neutrino energy 1.04( $\{13\}$ ) keV is ultra-low, further high-precision measurements of the excitation energy of the state are required. The parity of the 1683.0(10) keV state needs to be determined to verify the decay type of the transition to this state. The gs-to-gs  $Q$  value of  $^{95}\text{Tc}$  is now well refined to sub-keV uncertainty, combined with the energy level of 1675.40-keV state, an ultra-low distance (0.47 keV) of  $Q_{\text{EC}}^*$  to the computed atomic relaxation energy following the electron capture  $\varepsilon_k = 20.054$  keV [51] is observed.

### 3. Theoretical predictions

In the following we employed two calculation methods in order to predict the transition half-life and the distribution of energy released in the decay, namely atomic many-electron Dirac–Hartree–Fock–Slater (DHFS) self-consistent method and the nuclear shell model many-nucleon framework. The DHFS framework has been proven adequate for this type of calculations in our previous work [60].

Using the DHFS method we obtained the wave-functions and the energy levels of the atomic electrons. The calculations were performed for both the initial atom and the final atom. The initial atom was in its ground state. For the final atom, we considered all possible states with the electron configuration of the initial atom having a hole in each shell from which the electron could be captured. We assumed a central field  $V(r)$  for the atomic system. The potential has three components as given in [61]:

$$V_{\text{DHFS}}(r) = V_{\text{nuc}}(r) + V_{\text{el}}(r) + V_{\text{ex}}(r), \quad (2)$$

where  $V_{\text{nuc}}(r)$ ,  $V_{\text{el}}(r)$ ,  $V_{\text{ex}}(r)$  are the nuclear, electronic and exchange potential. The nuclear potential takes into account a realistic Fermi charge distribution in the nucleus [62]. The electronic potential is generated based on the charge distribution of the entire electron cloud. The procedure is iterative: after solving for the wave functions of the electrons, the charge distribution is recalculated and thus the potential as well. Then the computation is restarted until convergence. The exchange potential assures the correct asymptotic behaviour of the potential at  $r \rightarrow \infty$ . For the atomic structure calculations we made use of the RADIAL subroutine package [61], which also contains the DHFS.F code.

We denote the electron states as  $|(n, \kappa)\rangle$ , where  $n$  is the principal quantum number and  $\kappa$  is the relativistic quantum number. The atomic relaxation energy following the capture of an electron from the  $x = (n, \kappa)$  shell is denoted as  $\varepsilon_x$ . The values for  $\varepsilon_x$  are calculated according to the refined energy conservation in [60]:

$$\varepsilon_x = |T_{\text{g.s.}}| - |T_x|, \quad (3)$$

where  $T_{\text{g.s.}}$  and  $T_x$  are the total binding energy of the final atom in the ground state and in the excited state with a hole in the  $x$  shell.

For allowed transitions the energy distribution of an EC event is calculated as a sum over all atomic shells with  $\kappa = \pm 1$  as

$$\rho(E) = \frac{G_\beta^2}{(2\pi)^2} C \sum_x n_x \beta_x^2 B_x S_x p_v E_v \frac{\Gamma_x/(2\pi)}{(E - \varepsilon_x)^2 + \Gamma_x^2/4}, \quad (4)$$

where  $B_x$  and  $S_x$  are the exchange and overlap corrections, and the shake-up and shake-off corrections, respectively, as discussed in the following subsections. Here we go beyond

the formalism used in [27] by adding the shake-up and shake-off corrections into the energy distribution  $\rho(E)$ . Here  $E$  is related to the energy of the neutrino  $E_\nu$  and the  $Q$  value as  $E = Q_{\text{EC}}^* - E_\nu$ . The momentum of the neutrino is denoted as  $p_\nu = \sqrt{E_\nu^2 - m_\nu^2}$ . The Coulomb amplitude is represented as  $\beta_x$ , while  $n_x$  is the relative occupancy of the shell. The intrinsic line-widths of Breit–Wigner resonances centered at  $\varepsilon_x$  are denoted as  $\Gamma_x$  and are taken from [63]. The Fermi constant  $G_F$  and the Cabibbo angle  $\theta_C$  are combined in  $G_\beta = G_F \cos \theta_C$ . The nuclear structure information is contained in the shape factor  $C$  in terms of the nuclear form factor  ${}^A F_{101}^{(0)}$  [64]:

$$C = \left[ {}^A F_{101}^{(0)} \right]^2 = \left[ -\frac{g_A}{\sqrt{2J_i + 1}} M_{\text{GT}} \right]^2, \quad (5)$$

where  $M_{\text{GT}}$  is the Gamow–Teller nuclear matrix element [65]. The angular momentum of the initial nucleus is denoted as  $J_i$ , while the strength of the weak axial coupling is represented as  $g_A$ . For this calculation, we took values for  $g_A$  in the conservative interval 0.7 to 1 [66, 67, 68] and present the partial half-life corresponding to the mean decay rate in Table 3. The mean rate corresponds to a  $g_A$  value equal to 0.857. The half-life values for all  $g_A$  are between –33.3% and +36.1% of each mean value.

We define  $\lambda(E)$  as the total decay probability in the interval  $(0, E)$ :

$$\lambda(E) = \int_0^E \rho(E') dE' \quad (6)$$

and the total decay constant is calculated as  $\lambda \equiv \lambda(Q_{\text{EC}}^* - m_\nu)$ . After integration, using the narrow-width approximation, the decay rate can be written as

$$\lambda = \sum_x \lambda_x, \quad (7)$$

with the partial decay constant defined as

$$\lambda_x = \frac{G_\beta^2}{(2\pi)^2} C n_x \beta_x^2 B_x S_x p_{vx} (Q_{\text{EC}}^* - \varepsilon_x), \quad (8)$$

$$\text{where } p_{vx} = \sqrt{(Q_{\text{EC}}^* - \varepsilon_x)^2 - m_\nu^2}.$$

While an electron is captured by the nucleus, the other electrons (the spectator electrons) can undergo some processes which affect the decay rate. In the following subsections we will present a couple of corrections related to those processes.

#### 3.1. Exchange and overlap corrections

In the lowest-order approximation of the EC-decay process an electron is captured from an atomic shell  $x$  by the nucleus and a hole in this atomic shell is observed. However, the electrons are identical particles and one cannot distinguish between them leading to the possibility of a higher-order process where first an electron is captured from shell  $y$ ,

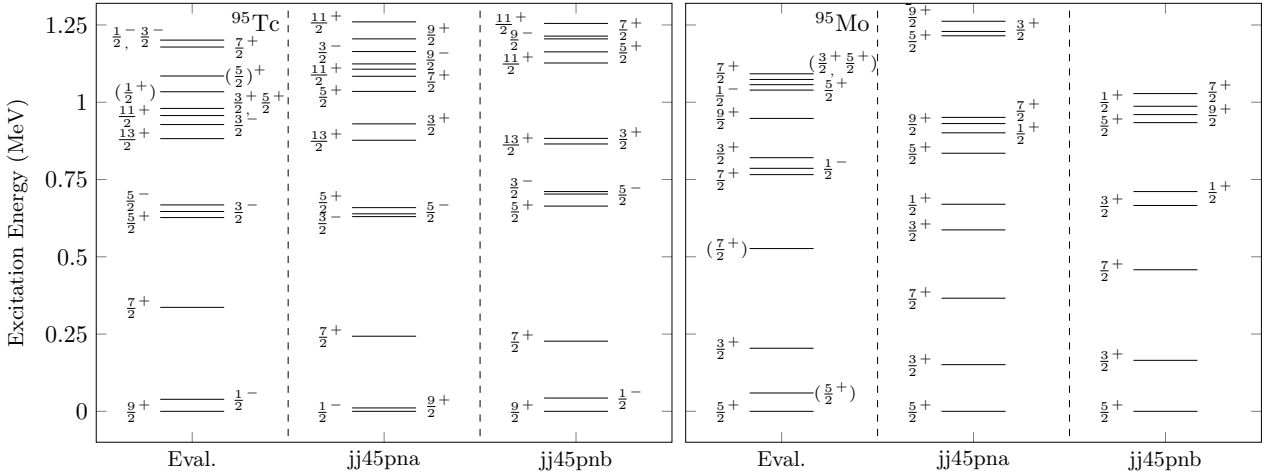


**Figure 3:** Computed level schemes of  $^{95}\text{Tc}$  and its daughter  $^{95}\text{Mo}$  using the Hamiltonians  $jj45pna$  and  $jj45pnb$ . A comparison with the available data is performed with the parentheses denoting uncertainty in parity and spin-parity assignments. The evaluated experimental energies are gathered from [50].

different from  $x$ , and simultaneously an electron from shell  $x$  is promoted to shell  $y$  and, again, the hole is observed in shell  $x$ . In both situations the hole appears in the same atomic shell, thus making those two paths for the EC decay indistinguishable from one another. The related higher-order correction is called the exchange correction.

After the EC decay the atomic number of the nucleus decreases by one unit and a hole is left in the daughter nucleus. Those changes affect the spectator electrons and thus their initial  $| (m, \kappa) \rangle$  and final  $| (m, \kappa)' \rangle$  wave functions do not perfectly overlap anymore, i.e.,  $\langle (m, \kappa)' | (m, \kappa) \rangle \neq 1$ . We use here the generalized formula from [69]:

$$B_{n\kappa} = \left| \frac{b_{n\kappa}}{\beta_{n\kappa}} \right|^2, \quad (9)$$

where  $\beta_{n\kappa}$  is the previously mentioned Coulomb amplitude, and

$$b_{n\kappa} = \left[ \prod_{m,\mu} \langle (m, \mu)' | (m, \mu) \rangle^{n_{m\mu}} \right] \langle (n, \kappa)' | (n, \kappa) \rangle^{-\frac{1}{2|\kappa|}} \times \left[ \beta_{n\kappa} - \sum_{m \neq n} \beta_{mk} \frac{\langle (m, \kappa)' | (n, \kappa) \rangle}{\langle (m, \kappa)' | (m, \kappa) \rangle} \right]. \quad (10)$$

This higher-order correction is called the overlap correction.

### 3.2. Shake-up and shake-off effects

During the EC decay, a spectator electron can be promoted to upper unoccupied shells, and this process is called the shake-up effect. The spectator electron can also be ejected to the continuum, and this process is called the shake-off effect. We consider a maximum of one spectator electron undergoing this transition, such that in the final state we would have at most two holes in the atomic shell. We use the formalism developed in [69] to end up with the following expression for the  $S_x$  factor of Eq. (4)

$$S_{n\kappa} = 1 + \sum_{m,\mu} P_{m\mu}. \quad (11)$$

Here  $P_{m\mu}$  represents the probability that a spectator electron from  $| (m, \mu) \rangle$  undergoes the shake-up or shake-off process. A spectator electron can remain in the initial shell, can swap shells with another spectator electron or be promoted or ejected. Thus  $P_{m\mu}$  can be computed as unity minus the probability for the electron to remain in the initial shell and the probability to swap shells, as

$$P_{m\mu} = 1 - |\langle (m, \mu)' | (m, \mu) \rangle|^{2n_{m\mu}} - \sum_{l \neq m} n'_{l\mu} n_{m\mu} |\langle (l, \mu)' | (m, \mu) \rangle|^2, \quad (12)$$

where  $n_x$  represents the occupancy of the shell  $x$ .

We also computed the impact of the two corrections on our theoretical calculations. Both the exchange and overlap corrections and the shake-up and shake-off effects increase the total decay rate by 8.1% and 8.6%, respectively. The impact of exchange and overlap corrections is 7.5% and 7.8%. In comparison, the shake-up and shake-off effects account for 0.61% and 0.64%. The first value in each pair of numbers refers to the decay corresponding to  $Q_{\text{EC}}^* = 20.52$  keV while the second one refers to  $Q_{\text{EC}}^* = 12.9$  keV. This increase in the decay rate is the result of the fact that both corrections open new channels for the decay process.

### 3.3. Nuclear Matrix Elements

For the nuclear-structure calculation we employed the *NuShellX@MSU* [74] code using the shell-model formalism. We used interactions *jj45pna* [75], a two-nucleon potential with a perturbative G-matrix approach with the single particle energies adjusted in the Coulomb part to reproduce the recent results in [76] and *jj45pnb* [77], both

**Table 2**

Comparison of the experimental excitation energies  $E_{\text{exc}}$  (measured in keV), electric quadrupole moments  $Q$  (measured in ebarns), and magnetic dipole moments  $\mu$  (measured in nuclear magnetons,  $\mu_N$ ), with those computed by the NSM using the *jj45pna*, *jj45pnb*, and *glekpn* Hamiltonians. The experimental evaluated energies are sourced from [50] and the nuclear moments from [70, 71, 72, 73]. The calculations employed effective charges of  $e_{\text{eff}}^p = 1.5e$  for protons and  $e_{\text{eff}}^n = 0.5e$  for neutrons, and the bare g-factors  $g_i(p) = 1$ ,  $g_i(n) = 0$ ,  $g_s(p) = 5.585$ , and  $g_s(n) = -3.826$  were used for determining the nuclear moments.

Isotope ( $J^\pi$ )	Experimental Evaluation			jj45pna			jj45pnb			glekpn		
	$E_{\text{exc}}$ (keV)	$Q$ (ebarn)	$\mu$ ( $\mu_N$ )									
$^{95}\text{Tc}$ ( $\frac{9}{2}^+$ )	0	-	5.94(6)	11	-0.1392	6.3286	0	-0.1508	6.3342	0	0.0784	6.3127
$^{95}\text{Mo}$ ( $\frac{5}{2}^+$ )	0	-0.022(1)	-0.9132(3)	0	-0.0379	-0.9418	0	-0.0238	-0.9768	574	-0.3359	-0.8376
$^{95}\text{Mo}$ ( $\frac{3}{2}^+$ )	204	-	-0.404(12)	151	0.0672	-0.0734	165	0.0656	-0.1335	816	-0.0782	0.6095

sharing the same jj45pn model space consisting of the proton  $0f_{5/2}-1p_{3/2}-1p_{1/2}-1g_{9/2}$  orbitals and the neutron  $0g_{7/2}-1d_{5/2}-1d_{3/2}-2s_{1/2}-0h_{11/2}$  orbitals with no truncations. Additionally, we employed the *glekpn* [78] interaction with the model space consisting of  $0f_{7/2}-0f_{5/2}-1p_{3/2}-1p_{1/2}-1g_{9/2}$  proton orbitals and  $0g_{9/2}-0g_{7/2}-1d_{5/2}-1d_{3/2}-2s_{1/2}$  neutron orbitals. For this model space, we applied truncations by fixing the occupation of the  $0f_{7/2}$  proton orbital to 8 protons and the  $0g_{9/2}$  neutron orbital to 10 neutrons, resulting in a shell-model closed core up to the magic numbers 28 for protons and 50 for neutrons. Lastly, for this interaction three sets of single-particle energies are available, we utilized the one suitable for the mass region  $A = 94 - 98$ . To assess the validity of the applied interactions, we have computed the energy-level schemes for both jj45pn model-space interactions as can be seen in Figure 3. The *glekpn* interaction did not reproduce the level schemes correctly so that the related energy spectrum is not shown here. The results indicate that the *jj45pnb* interaction provides better agreement with the evaluated data.

Further, we have compared the nuclear moments obtained using the three interactions with available evaluated experimental data, as presented in Table 2. Both the *jj45pna* and *jj45pnb* interaction showed a higher level of agreement with the observed values, showcasing their applicability and efficiency for the current study, whereas the Hamiltonian *glekpn* performs quite poorly. Nevertheless, engaging the *glekpn* interaction demonstrates the importance of exploring different interactions to fully understand their performance and limitations in this nuclear mass region.

### 3.4. Results of the calculations

We computed the energy levels of the daughter nucleus to identify the theoretical states corresponding to the experimental states of interest (1675.4 keV, 1683 keV). We compared the theoretical energies with the experimental ones and concluded that the following are the theoretical states closest to the experimental ones: for the experimental state with  $J_f = 9/2$  and  $E^* = 1675.4$  keV the best matches were  $E_{\text{th}}^* = 1748$  keV for *jj45pna*,  $E_{\text{th}}^* = 1897$  keV for *jj45pnb*, and  $E_{\text{th}}^* = 1703$  keV for *glekpn*. All the mentioned theoretical states have  $J_f = 9/2$ . For the experimental state having the energy  $E^* = 1683$  keV and with the angular

momentum and parity uncertain  $\{7/2^+, 9/2^+\}$ , the closest correspondence is for *jj45pna* the energy  $E_{\text{th}}^* = 1584$  keV, for *jj45pnb* the energy  $E_{\text{th}}^* = 1642$  keV, and for *glekpn* the energy  $E_{\text{th}}^* = 1707$  keV. The mentioned three theoretical states have the angular momentum and parity  $7/2^+$ .

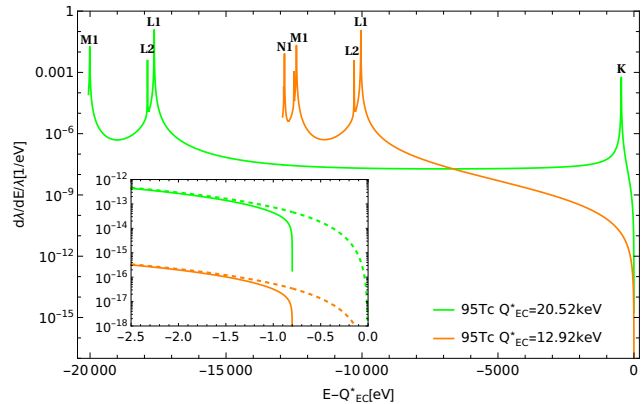


**Figure 4:** Normalized distributions of released energy in the EC decay of  $^{95}\text{Tc}$  in the transitions to the excited states of  $^{95}\text{Mo}$ , as functions of  $E - Q_{\text{EC}}^*$ . The experimental excitation energies are  $E^* = 1675.40$  keV and  $E^* = 1683.0$  keV, while the corresponding  $Q$  values are  $Q_{\text{EC}}^* = 20.52$  keV (green) and  $Q_{\text{EC}}^* = 12.9$  keV (orange). The K, L1, L2, M1 and N1 notations indicate sub-shells from which the electron was captured. The M2, N2 and O1 sub-shells are harder to distinguish and are not labeled. The inset indicates an enlarged endpoint region showing the effect of neutrino masses of 0.8 eV and 0 eV. The dotted lines depict the spectra for a massless neutrino, while the solid lines correspond to a neutrino mass of 0.8 eV.

In Table 3, we present the predicted half-lives for the decay of  $^{95}\text{Tc}$  to the two excited states of  $^{95}\text{Mo}$  with the experimental energies  $E^* = 1675.4$  keV and  $E^* = 1683$  keV for all relevant atomic shells and in Fig. 4, the normalized distribution of the released energy in the EC decay of  $^{95}\text{Tc}$  to excited states of  $^{95}\text{Mo}$  is demonstrated. The transition spectrum of  $^{95}\text{Tc}$  ( $9/2^+$ )  $\rightarrow$   $^{95}\text{Mo}^*$  (1675.4 keV) is indicated in green, with  $Q_{\text{EC}}^*$  of 20.52 keV, situated 0.47 keV relative to the computed atomic relaxation energy following the electron capture in the allowed K shell. In contrast, the transition  $^{95}\text{Tc}$  ( $9/2^+$ )  $\rightarrow$   $^{95}\text{Mo}^*$  (1683.0 keV), shown in orange, with a  $Q_{\text{EC}}^*$  value of 12.9 keV, is relatively farther

**Table 3**

Computed mean half-lives using  $g_A = 0.857$  (see the main text) for the EC decay of  $^{95}\text{Tc}$  to the two excited states in  $^{95}\text{Mo}$  (with experimental energies  $E^* = 1675.4$  keV and 1683 keV), using three shell-model interactions for the Gamow-Teller matrix element, with their experimental  $Q$  values shown in column 1. The second column indicates the used interactions and the third column the Gamow-Teller nuclear matrix element [65]. The computed total half-life and partial half-lives are demonstrated in columns 4-12. The atomic subshells are denoted using the X-ray notation.

$Q_{\text{EC}}^*$ (keV)	interaction	$M_{\text{GT}}$	Total half-life ( $10^3$ yr)	K ( $10^7$ yr)	L1 ( $10^4$ yr)	L2 ( $10^5$ yr)	M1 ( $10^4$ yr)	M2 ( $10^6$ yr)	N1 ( $10^5$ yr)	N2 ( $10^7$ yr)	O1 ( $10^6$ yr)
20.52	jj45pna	-0.00696	877	20.0	117	708	640	267	223	146	491
	jj45pnb	-0.016533	155	3.55	20.8	125	81.6	47.4	39.4	25.8	87.1
	glekpn	0.0070667	850	19.4	114	587	446	259	216	141	477
12.9	jj45pna	-0.02412	173	-	24.1	143	79.7	46.0	37.5	24.5	82.6
	jj45pnb	-0.0198667	255	-	35.6	210	117	67.9	55.3	36.1	122
	glekpn	0.2296	1.9	-	0.266	1.57	0.880	0.508	0.414	0.271	0.911

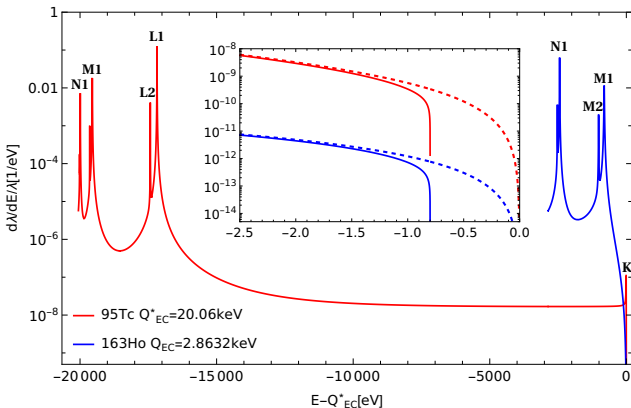


**Figure 5:** Normalized distribution of released energy in the EC decay of  $^{95}\text{Tc}$  in the transition to the excited state  $E^* = 1675.40$  keV of  $^{95}\text{Mo}$ , with  $Q_{\text{EC}}^* = 20.06$  keV, as function of  $E - Q_{\text{EC}}^*$  in comparison to that of  $^{163}\text{Ho}$  with gs-to-gs  $Q_{\text{EC}} = 2.8632$  keV [79]. The red line corresponds to the on-resonance EC decay using the experimental  $Q_{\text{EC}}^*$  of 20.06 keV within  $1\sigma$  range of the central value 20.52 keV, while the blue line corresponds to the  $Q_{\text{EC}}^*$  of 2.8632 keV. For the sub-shell notation and the inset the reader is referred to the caption of Fig. 4

from the computed atomic relaxation energy following the electron capture of the allowed L1 shell (giving a value of 10 keV for the distance). As illustrated in the inset of Fig. 4, a more pronounced resonance enhancement in the last 0.8 eV region near the endpoint for the former transition is observed, suggesting a preference for choosing this transition as a candidate for determining a non-vanishing neutrino mass. This phenomenon guides us to search for cases that have the smallest distance of  $Q_{\text{EC}}^*$  to the highest ionization energy of the captured electron of all allowed shells for neutrino-mass determination experiments.

The decay rate close to the endpoint is highly sensitive to small variations of the  $Q$  value as demonstrated by the 1s level, K, manifesting as a resonance itself, and thus can radically increase the number of recorded events near the endpoint. The current accuracy of measurement of the  $Q_{\text{EC}}^*$  value does not allow to make an unambiguous conclusion about the position of the 1s level, relative to the endpoint. Assuming  $Q_{\text{EC}}^* = 20.06$  keV, which is consistent with the

$1\sigma$  range of experimental error and is shifted by -0.46 keV relative to the central value, the resonance at the endpoint provides the highest EC event rate in the neutrino-mass sensitive region. Figure 5 shows the normalized EC energy spectrum as a function of the energy,  $E - Q_{\text{EC}}^*$ , deposited in a calorimeter through the de-excitation of atomic shells for  $Q_{\text{EC}}^* = 20.06$  keV, in comparison to the EC energy spectra in  $^{163}\text{Ho}$  atom. The s1 level, K, has a significant EC counting-rate enhancement for the transition  $^{95}\text{Tc} (9/2^+) \rightarrow {}^{95}\text{Mo}^* (1675.40 \text{ keV})$  in the neutrino-mass sensitive region, as shown on an enlarged scale in the inset of Fig. 5. Assuming a  $Q$  value of  $Q_{\text{EC}}^* = 20.06$  keV, technetium is about three orders of magnitude more effective than holmium. Based on these findings, it can be conjectured that we have found a potentially strong transition for direct electron-neutrino mass determination. However, the short half-life of about 1 day for the  $^{95}\text{Tc}$  can prove to be a challenge experimentally.

#### 4. Conclusion and outlook

A direct high-precision gs-to-gs EC-decay  $Q$ -value measurement of  $^{95}\text{Tc} (9/2^+) \rightarrow {}^{95}\text{Mo} (5/2^+)$  was performed using the PI-ICR technique at the JYFLTRAP Penning trap mass spectrometer. A  $Q$  value of  $1695.92(13)$  keV was obtained and the precision was improved by a factor of around 37 compared to literature. The measurement also improved the mass excess of  $^{95}\text{Tc}$  by a factor of 28 compared to previous experiments. Three candidate transitions of  $^{95}\text{Tc} (9/2^+) \rightarrow {}^{95}\text{Mo}^*$  were validated to be energetically allowed. The refined sub-keV precision of the gs-to-gs  $Q$  value of  $^{95}\text{Tc}$  allows us to find an ultra-low energy difference (0.47 keV) between  $Q_{\text{EC}}^*$  and the atomic relaxation energy  $\epsilon_k = 20.054$  keV in the K capture for the allowed gs-to-es transition to the 1675.40-keV state. The spin of the 1683.0-keV state needs to be determined along with its energy with higher precision in order to see if the related transition is allowed and of low  $Q$  value.

The atomic self-consistent many-electron Dirac–Hartree–Fock–Slater method and three nuclear shell-model interactions were utilized to predict the partial decay half-lives and energy distributions of gs-to-es EC transitions in  $^{95}\text{Tc}$  with low  $Q$  values. We computed the energy levels of the parent

and daughter nuclei and a few electromagnetic moments to assess the validity of the three shell-model interactions ( $jj45pn\alpha$ ,  $jj45pn\beta$ ,  $glekpn$ ). Multiple corrections, such as exchange, overlap, shake-up, and shake-off effects, were accounted for in these predictions. From the calculations, the ultra-low distance to the atomic line K, level 1s, for  $^{95}\text{Tc}$  ( $9/2^+$ )  $\rightarrow$   $^{95}\text{Mo}^*$  (1675.40 keV) results in a significant increase in the number of EC events in the energy region sensitive to the electron neutrino mass. These findings confirm a potentially powerful transition for direct electron-neutrino mass determination.

## References

- Fukuda, Y., Hayakawa, T., Ichihara, E., Inoue, K., Ishihara, K., Ishino, H., Itow, Y., Kajita, T., Kameda, J., Kasuga, S., Kobayashi, K., Kobayashi, Y., Koshio, Y., Miura, M., Nakahata, M., Nakayama, S., Okada, A., Okumura, K., Sakurai, N., Shiozawa, M., Suzuki, Y., Takeuchi, Y., Totsuka, Y., Yamada, S., Earl, M., Habig, A., Kearns, E., Messier, M.D., Scholberg, K., Stone, J.L., Sulak, L.R., Walter, C.W., Goldhaber, M., Barszczak, T., Casper, D., Gajewski, W., Halverson, P.G., Hsu, J., Kropp, W.R., Price, L.R., Reines, F., Smy, M., Sobel, H.W., Vagins, M.R., Ganezer, K.S., Keig, W.E., Ellsworth, R.W., Tasaka, S., Flanagan, J.W., Kibayashi, A., Learned, J.G., Matsuno, S., Stenger, V.J., Takemori, D., Ishii, T., Kanzaki, J., Kobayashi, T., Mine, S., Nakamura, K., Nishikawa, K., Oyama, Y., Sakai, A., Sakuda, M., Sasaki, O., Echigo, S., Kohama, M., Suzuki, A.T., Haines, T.J., Blaufuss, E., Kim, B.K., Sanford, R., Svoboda, R., Chen, M.L., Conner, Z., Goodman, J.A., Sullivan, G.W., Hill, J., Jung, C.K., Martens, K., Mauger, C., Mc Grew, C., Sharkey, E., Viren, B., Yanagisawa, C., Doki, W., Miyano, K., Okazawa, H., Saji, C., Takahata, M., Nagashima, Y., Takita, M., Yamaguchi, T., Yoshida, M., Kim, S.B., Etoh, M., Fujita, K., Hasegawa, A., Hasegawa, T., Hatakeyama, S., Iwamoto, T., Koga, M., Maruyama, T., Ogawa, H., Shirai, J., Suzuki, A., Tsushima, F., Koshiba, M., Nemoto, M., Nishijima, K., Futagami, T., Hayato, Y., Kanaya, Y., Kaneyuki, K., Watanabe, Y., Kielczewska, D., Doyle, R.A., George, J.S., Stachyra, A.L., Wai, L.L., Wilkes, R.J., Young, K.K.. Evidence for oscillation of atmospheric neutrinos. *Physical Review Letters* 1998;81(8):1562–1567. URL: <http://link.aps.org/doi/10.1103/PhysRevLett.81.1562>. arXiv:9807003. doi:10.1103/PhysRevLett.81.1562.
- SNO Collaboration, . Direct Evidence for Neutrino Flavor Transformation from Neutral-Current Interactions in the Sudbury Neutrino Observatory. *Physical Review Letters* 2002;89(1):1–6. URL: <http://dx.doi.org/10.1103/PhysRevLett.89.011301>. doi:10.1103/PhysRevLett.89.011301. arXiv:0204008.
- Gerbino, M., Lattanzi, M.. Status of neutrino properties and future prospects—cosmological and astrophysical constraints. *Frontiers in Physics* 2018;5. doi:10.3389/fphy.2017.00070.
- Giusarma, E., Reyes, M., Villaescusa-Navarro, F., He, S., Ho, S., Hahn, C.. Learning neutrino effects in cosmology with convolutional neural network. *The Astrophysical Journal* 2023;950(1):70. URL: <https://dx.doi.org/10.3847/1538-4357/accd61>. doi:10.3847/1538-4357/accd61.
- Suhonen, J., Civitarese, O.. Weak-interaction and nuclear-structure aspects of nuclear double beta decay. *Physics Reports* 1998;300(3-4):123–214. URL: [http://dx.doi.org/10.1016/S0370-1573\(97\)00087-2](http://dx.doi.org/10.1016/S0370-1573(97)00087-2). doi:10.1016/S0370-1573(97)00087-2.
- Avignone, F.T., Elliott, S.R., Engel, J.. Double beta decay, Majorana neutrinos, and neutrino mass. *Reviews of Modern Physics* 2008;80(2):481–516. URL: <http://link.aps.org/doi/10.1103/RevModPhys.80.481>. doi:10.1103/RevModPhys.80.481. arXiv:0708.1033.
- Ejiri, H., Suhonen, J., Zuber, K.. Neutrino–nuclear responses for astro-neutrinos, single beta decays and double beta decays. *Physics Reports* 2019;797:1–102. URL: <https://doi.org/10.1016/j.physrep.2018.12.001>. doi:10.1016/j.physrep.2018.12.001.
- Agostini, M., Benato, G., Detwiler, J.A., Menéndez, J., Vissani, F.. Toward the discovery of matter creation with neutrinoless  $\beta\beta$  decay. *Rev Mod Phys* 2023;95:025002. URL: <https://link.aps.org/doi/10.1103/RevModPhys.95.025002>. doi:10.1103/RevModPhys.95.025002.
- Drexlin, G., Hannen, V., Mertens, S., Weinheimer, C.. Current direct neutrino mass experiments. *Advances in High Energy Physics* 2013;2013(i):1–39. URL: <http://www.hindawi.com/journals/ahep/2013/293986/>. doi:10.1155/2013/293986. arXiv:1307.0101.
- Aker, M., Altenmüller, K., Arenz, M., Babutzka, M., Barrett, J., Bauer, S., Beck, M., Beglarian, A., Behrens, J., Bergmann, T., Besserer, U., Blaum, K., Block, F., Bobien, S., Bokeloh, K., Bonn, J., Bornschein, B., Bornschein, L., Bouquet, H., Brunst, T., Caldwell, T.S., La Cascio, L., Chilingaryan, S., Choi, W., Corona, T.J., Debowski, K., Deffert, M., Descher, M., Doe, P.J., Dragoun, O., Drexlin, G., Dunmore, J.A., Dyba, S., Edzards, F., Eisenblätter, L., Eitel, K., Ellinger, E., Engel, R., Enomoto, S., Erhard, M., Eversheim, D., Fedkevych, M., Felden, A., Fischer, S., Flatt, B., Formaggio, J.A., Fränkle, F.M., Franklin, G.B., Frankrone, H., Friedel, F., Fuchs, D., Fulst, A., Furse, D., Gauda, K., Gemmeke, H., Gil, W., Glück, F., Görhardt, S., Groh, S., Grohmann, S., Grössle, R., Gumbsheimer, R., Ha Minh, M., Hackenjos, M., Hannen, V., Harms, F., Hartmann, J., Haußmann, N., Heizmann, F., Helbing, K., Hickford, S., Hilk, D., Hillen, B., Hillesheimer, D., Hinz, D., Höhn, T., Holzapfel, B., Holzmann, S., Houdy, T., Howe, M.A., Huber, A., James, T.M., Jansen, A., Kaboth, A., Karl, C., Kazachenko, O., Kellerer, J., Kernert, N., Kippenbrock, L., Kleesiek, M., Klein, M., Köhler, C., Köllenberger, L., Kopmann, A., Korzeczek, M., Kosmider, A., Kováčik, A., Krasch, B., Kraus, M., Krause, H., Kuckert, L., Kuffner, B., Kunka, N., Lasserre, T., Le, T.L., Lebeda, O., Leber, M., Lehnert, B., Letnev, J., Leven, F., Lichter, S., Lobashev, V.M., Lokhov, A., MacHatschek, M., Malcherek, E., Müller, K., Mark, M., Marsteller, A., Martin, E.L., Melzer, C., Menshikov, A., Mertens, S., Minter, L.I., Mirz, S., Monreal, B., Morales Guzmán, P.I., Müller, K., Naumann, U., Ndeke, W., Neumann, H., Niemes, S., Noe, M., Oblath, N.S., Ortjohann, H.W., Osipowicz, A., Ostrick, B., Otten, E., Parno, D.S., Phillips, D.G., Plischke, P., Pollithy, A., Poon, A.W., Pouryamout, J., Prall, M., Priester, F., Röllig, M., Rötteler, C., Ranitzsch, P.C., Rest, O., Rinderspacher, R., Robertson, R.G., Rodenbeck, C., Rohr, P., Roll, C., Rupp, S., Ryšavý, M., Sack, R., Saenz, A., Schäfer, P., Schimpf, L., Schlösser, K., Schlösser, M., Schlüter, L., Schön, H., Schönung, K., Schrank, M., Schulz, B., Schwarz, J., Seitz-Moskaliuk, H., Seller, W., Sibile, V., Siegmund, D., Skasyrskaya, A., Slezák, M., Špalek, A., Spanier, F., Steidl, M., Steinbrink, N., Sturm, M., Suesser, M., Sun, M., Tcherniakhovski, D., Telle, H.H., Thümmler, T., Thorne, L.A., Titov, N., Tkachev, I., Trost, N., Urban, K., Vénos, D., Valerius, K., Vandevender, B.A., Vianden, R., Vizcaya Hernández, A.P., Wall, B.L., Wüstling, S., Weber, M., Weinheimer, C., Weiss, C., Welte, S., Wendel, J., Wierman, K.J., Wilkerson, J.F., Wolf, J., Xu, W., Yen, Y.R., Zacher, M., Zadorozhny, S., Zbořil, M., Zeller, G.. Improved Upper Limit on the Neutrino Mass from a Direct Kinematic Method by KATRIN. *Physical Review Letters* 2019;123(22):1–11. URL: <https://doi.org/10.1103/PhysRevLett.123.221802>. doi:10.1103/PhysRevLett.123.221802. arXiv:1909.06048.
- Aker, M., Beglarian, A., Behrens, J., Berlev, A., Besserer, U., Bieringer, B., Block, F., Bornschein, B., Bornschein, L., Böttcher, M., Brunst, T., Caldwell, T.S., Carney, R.M.D., Cascio, L.L., Chilingaryan, S., Choi, W., Debowski, K., Deffert, M., Descher, M., Barrero, D.D., Doe, P.J., Dragoun, O., Drexlin, G., Eitel, K., Ellinger, E., Engel, R., Enomoto, S., Felden, A., Formaggio, J.A., Fränkle, F.M., Franklin, G.B., Friedel, F., Fulst, A., Gauda, K., Gil, W., Glück, F., Grössle, R., Gumbsheimer, R., Gupta, V., Höhn, T., Hannen, V., Haußmann, N., Helbing, K., Hickford, S., Hiller, R., Hillesheimer, D., Hinz, D., Houdy, T., Huber, A., Jansen, A., Karl,

- C., Kellerer, F., Kellerer, J., Klein, M., Köhler, C., Köllenberger, L., Kopmann, A., Korzeczek, M., Kovalík, A., Krasch, B., Krause, H., Kunka, N., Lasserre, T., Le, T.L., Lebeda, O., Lehner, B., Lokhov, A., Machatschek, M., Malcherek, E., Mark, M., Marsteller, A., Martin, E.L., Melzer, C., Menshikov, A., Mertens, S., Mostafa, J., Müller, K., Niemes, S., Oelpmann, P., Parno, D.S., Poon, A.W.P., Poyato, J.M.L., Priester, F., Röllig, M., Röttel, C., Robertson, R.G.H., Rodejohann, W., Rodenbeck, C., Ryšavý, M., Sack, R., Saenz, A., Schäfer, P., Schaller, A., Schimpf, L., Schlösser, K., Schlösser, M., Schlüter, L., Schneidewind, S., Schrank, M., Schulz, B., Schwemmer, A., Šefčík, M., Sibille, V., Siegmann, D., Slezák, M., Steidl, M., Sturm, M., Sun, M., Tcherniakhovski, D., Telle, H.H., Thorne, L.A., Thümmler, T., Titov, N., Tkachev, I., Urban, K., Valerius, K., Vénos, D., Hernández, A.P.V., Weinheimer, C., Welte, S., Wendel, J., Wilkerson, J.F., Wolf, J., Wüstling, S., Xu, W., Yen, Y.R., Zadorogny, S., Zeller, G.. Direct neutrino-mass measurement with sub-electronvolt sensitivity. *Nature Physics* 2022;18:160. URL: <https://doi.org/10.1038/s41567-021-01463-1>. doi:<https://doi.org/10.1038/s41567-021-01463-1>.
12. Ashtari Esfahani, A., Böser, S., Buzinsky, N., Carmona-Benitez, M.C., Claessens, C., de Viveiros, L., Doe, P.J., Fertl, M., Formaggio, J.A., Gaison, J.K., Gladstone, L., Grando, M., Guigue, M., Hartse, J., Heeger, K.M., Huyan, X., Johnston, J., Jones, A.M., Kazkaz, K., LaRoque, B.H., Li, M., Lindman, A., Machado, E., Marsteller, A., Matthé, C., Mohiuddin, R., Montreal, B., Mueller, R., Nikkel, J.A., Novitski, E., Oblath, N.S., Peña, J.I., Pettus, W., Reimann, R., Robertson, R.G.H., Rosa De Jesús, D., Rybka, G., Saldaña, L., Schram, M., Slocum, P.L., Stachurska, J., Sun, Y.H., Surukuchi, P.T., Tedeschi, J.R., Telles, A.B., Thomas, F., Thomas, M., Thorne, L.A., Thümmler, T., Tvrznikova, L., Van De Pontsele, W., VanDevender, B.A., Weintroub, J., Weiss, T.E., Wendler, T., Young, A., Zayas, E., Ziegler, A. (Project 8 Collaboration). Tritium beta spectrum measurement and neutrino mass limit from cyclotron radiation emission spectroscopy. *Phys Rev Lett* 2023;131:102502. URL: <https://link.aps.org/doi/10.1103/PhysRevLett.131.102502>. doi:[10.1103/PhysRevLett.131.102502](https://doi.org/10.1103/PhysRevLett.131.102502).
13. Gastaldo, L., Blaum, K., Doerr, A., Düllmann, C.E., Eberhardt, K., Eliseev, S., Enss, C., Faessler, A., Fleischmann, A., Kempf, S., Krivoruchenko, M., Lahiri, S., Maiti, M., Novikov, Y.N., Ranitzsch, P.C., Simkovic, F., Szucs, Z., Wegner, M.. The electron capture  $^{163}\text{Ho}$  experiment ECHO. *Journal of Low Temperature Physics* 2014;176(5-6):876–884. URL: <http://dx.doi.org/10.1007/s10909-014-1187-4>. doi:[10.1007/s10909-014-1187-4](https://doi.org/10.1007/s10909-014-1187-4). arXiv:1306.2655.
14. Gastaldo, L., Blaum, K., Chrysalidis, K., Day Goodacre, T., Domula, A., Door, M., Dorrer, H., Düllmann, C.E., Eberhardt, K., Eliseev, S., Enss, C., Faessler, A., Filianin, P., Fleischmann, A., Fonnesu, D., Gamer, L., Haas, R., Hassel, C., Hengstler, D., Jochum, J., Johnston, K., Kebschull, U., Kempf, S., Kieck, T., Köster, U., Lahiri, S., Maiti, M., Mantegazzini, F., Marsh, B., Neroutsos, P., Novikov, Y.N., Ranitzsch, P.C., Rothe, S., Rischka, A., Saenz, A., Sander, O., Schneider, F., Scholl, S., Schüssler, R.X., Schweiger, C., Simkovic, F., Stora, T., Szucs, Z., Türler, A., Veinhard, M., Weber, M., Wegner, M., Wendt, K., Zuber, K.. The electron capture in  $^{163}\text{Ho}$  experiment – ECHO. *European Physical Journal: Special Topics* 2017;226(8):1623–1694. URL: <http://link.springer.com/10.1140/epjst/e2017-70071-y>. doi:[10.1140/epjst/e2017-70071-y](https://doi.org/10.1140/epjst/e2017-70071-y).
15. Velte, C., Ahrens, F., Barth, A., Blaum, K., Braß, M., Door, M., Dorrer, H., Düllmann, C.E., Eliseev, S., Enss, C., Filianin, P., Fleischmann, A., Gastaldo, L., Goeggelmann, A., Goodacre, T.D., Havercort, M.W., Hengstler, D., Jochum, J., Johnston, K., Keller, M., Kempf, S., Kieck, T., König, C.M., Köster, U., Kromer, K., Mantegazzini, F., Marsh, B., Novikov, Y.N., Piquemal, F., Riccio, C., Richter, D., Rischka, A., Rothe, S., Schüssler, R.X., Schweiger, C., Stora, T., Wegner, M., Wendt, K., Zampaolo, M., Zuber, K.. High-resolution and low-background  $^{163}\text{Ho}$  spectrum: interpretation of the resonance tails. *The European Physical Journal C* 2019;79(12). URL: <http://link.springer.com/10.1140/epjc/s10052-019-7513-x>. doi:[10.1140/epjc/s10052-019-7513-x](https://doi.org/10.1140/epjc/s10052-019-7513-x).
16. Mantegazzini, F., Kovac, N., Enss, C., Fleischmann, A., Griedel, M., Gastaldo, L.. Development and characterisation of high-resolution microcalorimeter detectors for the echo-100k experiment. *Nuclear Instruments and Methods in Physics Research Section A: Accelerators, Spectrometers, Detectors and Associated Equipment* 2023;1055:168564. URL: <https://www.sciencedirect.com/science/article/pii/S0168900223005545>. doi:<https://doi.org/10.1016/j.nima.2023.168564>.
17. Nucciotti, A., Alpert, B., Balata, M., Becker, D., Bennett, D., Bevilacqua, A., Biasotti, M., Ceriale, V., Ceruti, G., Corsini, D., De Gerone, M., Dressler, R., Faverzani, M., Ferri, E., Fowler, J., Gallucci, G., Gard, J., Gatti, F., Giachero, A., Hays-Wehle, J., Heinitz, S., Hilton, G., Köster, U., Lusignoli, M., Mates, J., Nisi, S., Orlando, A., Parodi, L., Pessina, G., Puiu, A., Ragazzi, S., Reintsema, C., Ribeiro-Gomez, M., Schmidt, D., Schuman, D., Siccardi, F., Swetz, D., Ullom, J., Vale, L.. Status of the HOLMES Experiment to Directly Measure the Neutrino Mass. *Journal of Low Temperature Physics* 2018;193(5-6):1137–1145. doi:[10.1007/s10909-018-2025-x](https://doi.org/10.1007/s10909-018-2025-x). arXiv:1807.09269.
18. Borghesi, M., Alpert, B., Balata, M., Becker, D., Bennet, D., Celasco, E., Cerboni, N., De Gerone, M., Dressler, R., Faverzani, M., Fedkevych, M., Ferri, E., Fowler, J., Gallucci, G., Gard, J., Gatti, F., Giachero, A., Hilton, G., Köster, U., Labranca, D., Lusignoli, M., Mates, J., Mauger, E., Nisi, S., Nucciotti, A., Origo, L., Pessina, G., Ragazzi, S., Reintsema, C., Schmidt, D., Schumann, D., Swetz, D., Ullom, J., Vale, L.. An updated overview of the holmes status. *Nuclear Instruments and Methods in Physics Research Section A: Accelerators, Spectrometers, Detectors and Associated Equipment* 2023;1051:168205. URL: <https://www.sciencedirect.com/science/article/pii/S016890022300195X>. doi:<https://doi.org/10.1016/j.nima.2023.168205>.
19. McDonald, A.B., Drexl, G., Hannen, V., Mertens, S., Weinheimer, C.. Current direct neutrino mass experiments. *Advances in High Energy Physics* 2013;2013:293986. URL: <https://doi.org/10.1155/2013/293986>. doi:[10.1155/2013/293986](https://doi.org/10.1155/2013/293986).
20. Ferri, E., Bagliani, D., Biasotti, M., Ceruti, G., Corsini, D., Faverzani, M., Gatti, F., Giachero, A., Gotti, C., Kilbourne, C., Kling, A., Maino, M., Manfrinetti, P., Nucciotti, A., Pessina, G., Pizzigoni, G., Ribeiro Gomes, M., Sisti, M.. The Status of the MARE Experiment with  $^{187}\text{Re}$  and  $^{163}\text{Ho}$  Isotopes. *Physics Procedia* 2015;61(August):227–231. URL: <http://dx.doi.org/10.1016/j.phpro.2014.12.037>. doi:[10.1016/j.phpro.2014.12.037](https://doi.org/10.1016/j.phpro.2014.12.037).
21. Haaranen, M., Suhonen, J.. Beta decay of  $^{115}\text{Cd}$  and its possible ultra-low  $Q$ -value branch. *The European Physical Journal A* 2013;49(7):1–9. URL: <http://dx.doi.org/10.1140/epja/i2013-13093-8>. doi:[10.1140/epja/i2013-13093-8](https://doi.org/10.1140/epja/i2013-13093-8).
22. Suhonen, J.. Theoretical studies of rare weak processes in nuclei. *Physica Scripta* 2014;89(5):54032. URL: <http://stacks.iop.org/1402-4896/89/i=5/a=054032>. doi:[10.1088/0031-8949/89/5/054032](https://doi.org/10.1088/0031-8949/89/5/054032).
23. Sandler, R., Bollen, G., Gamage, N.D., Hamaker, A., Izzo, C., Puentes, D., Redshaw, M., Ringle, R., Yandow, I.. Investigation of the potential ultralow  $Q$ -value  $\beta$ -decay candidates  $\text{Sr } 89$  and  $\text{Ba } 139$  using Penning trap mass spectrometry. *Physical Review C* 2019;100(2):1–5. URL: <https://link.aps.org/doi/10.1103/PhysRevC.100.024309>. arXiv:1906.03335.
24. Karthein, J., Atanasov, D., Blaum, K., Eliseev, S., Filianin, P., Lunney, D., Manea, V., Mougeot, M., Neidherr, D., Novikov, Y., Schweikhard, L., Welker, A., Wienholtz, F., Zuber, K.. Direct decay-energy measurement as a route to the neutrino mass. *Hyperfine Interactions* 2019;240(1):1–9. URL: <http://link.springer.com/10.1007/s10751-019-1601-z>. doi:[10.1007/s10751-019-1601-z](https://doi.org/10.1007/s10751-019-1601-z). arXiv:1905.05510.
25. De Roubin, A., Kostensalo, J., Eronen, T., Canete, L., De Groote, R.P., Jokinen, A., Kankainen, A., Nesterenko, D.A., Moore, I.D., Rinta-Antila, S., Suhonen, J., Vilén, M.. High-Precision  $Q$ -Value Measurement Confirms the Potential of  $\text{Cs } 135$  for Absolute Antineutrino Mass Scale Determination. *Physical Review Letters*

- 2020;124(22):1–5. URL: <https://doi.org/10.1103/PhysRevLett.124.222503>. doi:10.1103/PhysRevLett.124.222503. arXiv:2002.08282.
26. Ge, Z., Eronen, T., de Roubin, A., Nesterenko, D.A., Hukkanen, M., Beliuskina, O., de Groote, R., Geldhof, S., Gins, W., Kankainen, A., Koszorús, A., Kotila, J., Kostensalo, J., Moore, I.D., Raggio, A., Rinta-Antila, S., Suhonen, J., Virtanen, V., Weaver, A.P., Zadvornaya, A., Jokinen, A.. Direct measurement of the mass difference of  $^{72}\text{As}$ – $^{72}\text{Ge}$  rules out  $^{72}\text{As}$  as a promising  $\beta$ -decay candidate to determine the neutrino mass. *Physical Review C* 2021;103:065502. URL: <https://link.aps.org/doi/10.1103/PhysRevC.103.065502>. doi:10.1103/PhysRevC.103.065502.
  27. Ge, Z., Eronen, T., Tyrin, K.S., Kotila, J., Kostensalo, J., Nesterenko, D.A., Beliuskina, O., de Groote, R., de Roubin, A., Geldhof, S., Gins, W., Hukkanen, M., Jokinen, A., Kankainen, A., Koszorús, A., Krivoruchenko, M.I., Kujanpää, S., Moore, I.D., Raggio, A., Rinta-Antila, S., Suhonen, J., Virtanen, V., Weaver, A.P., Zadvornaya, A..  $^{159}\text{Dy}$  electron-capture: A new candidate for neutrino mass determination. *Phys Rev Lett* 2021;127:272301. URL: <https://link.aps.org/doi/10.1103/PhysRevLett.127.272301>. doi:10.1103/PhysRevLett.127.272301.
  28. Ge, Z., Eronen, T., de Roubin, A., Tyrin, K., Canete, L., Geldhof, S., Jokinen, A., Kankainen, A., Kostensalo, J., Kotila, J., Krivoruchenko, M., Moore, I., Nesterenko, D., Suhonen, J., Vilén, M.. High-precision electron-capture  $q$  value measurement of  $^{111}\text{In}$  for electron-neutrino mass determination. *Physics Letters B* 2022;832:137226. URL: <https://www.sciencedirect.com/science/article/pii/S0370269322003604>. doi:<https://doi.org/10.1016/j.physletb.2022.137226>.
  29. Eronen, T., Ge, Z., de Roubin, A., Ramalho, M., Kostensalo, J., Kotila, J., Beliuskina, O., Delafosse, C., Geldhof, S., Gins, W., Hukkanen, M., Jokinen, A., Kankainen, A., Moore, I., Nesterenko, D., Stryjczyk, M., Suhonen, J.. High-precision measurement of a low  $q$  value for allowed beta-decay of  $^{131}\text{I}$  related to neutrino mass determination. *Physics Letters B* 2022;830:137135. URL: <https://www.sciencedirect.com/science/article/pii/S0370269322002696>. doi:<https://doi.org/10.1016/j.physletb.2022.137135>.
  30. Ge, Z., Eronen, T., de Roubin, A., Kostensalo, J., Suhonen, J., Nesterenko, D.A., Beliuskina, O., de Groote, R., Delafosse, C., Geldhof, S., Gins, W., Hukkanen, M., Jokinen, A., Kankainen, A., Kotila, J., Koszorús, A., Moore, I.D., Raggio, A., Rinta-Antila, S., Virtanen, V., Weaver, A.P., Zadvornaya, A.. Direct determination of the atomic mass difference of the pairs  $^{76}\text{As}$ – $^{76}\text{Se}$  and  $^{155}\text{Tb}$ – $^{155}\text{Gd}$  rules out  $^{76}\text{As}$  and  $^{155}\text{Tb}$  as possible candidates for electron (anti)neutrino mass measurements. *Phys Rev C* 2022;106:015502. URL: <https://link.aps.org/doi/10.1103/PhysRevC.106.015502>. doi:10.1103/PhysRevC.106.015502.
  31. Ramalho, M., Ge, Z., Eronen, T., Nesterenko, D.A., Jaatinen, J., Jokinen, A., Kankainen, A., Kostensalo, J., Kotila, J., Krivoruchenko, M.I., Suhonen, J., Tyrin, K.S., Virtanen, V.. Observation of an ultralow- $q$ -value electron-capture channel decaying to  $^{75}\text{As}$  via a high-precision mass measurement. *Phys Rev C* 2022;106:015501. URL: <https://link.aps.org/doi/10.1103/PhysRevC.106.015501>. doi:10.1103/PhysRevC.106.015501.
  32. Gamage, N.D., Sandler, R., Buchinger, F., Clark, J.A., Ray, D., Orford, R., Porter, W.S., Redshaw, M., Savard, G., Sharma, K.S., Valverde, A.A.. Precise  $q$ -value measurements of  $^{112,113}\text{Ag}$  and  $^{115}\text{Cd}$  with the canadian penning trap for evaluation of potential ultralow  $q$ -value  $\beta$  decays. *Phys Rev C* 2022;106:045503. URL: <https://link.aps.org/doi/10.1103/PhysRevC.106.045503>. doi:10.1103/PhysRevC.106.045503.
  33. Kebilbeck, D.K., Bhandari, R., Gamage, N.D., Horana Gamage, M., Leach, K.G., Mougeot, X., Redshaw, M.. Updated evaluation of potential ultralow  $q$ -value  $\beta$ -decay candidates. *Phys Rev C* 2023;107:015504. URL: <https://link.aps.org/doi/10.1103/PhysRevC.107.015504>. doi:10.1103/PhysRevC.107.015504.
  34. Ge, Z., Eronen, T., de Roubin, A., Ramalho, M., Kostensalo, J., Kotila, J., Suhonen, J., Nesterenko, D.A., Kankainen, A., Ascher, P., Beliuskina, O., Flayol, M., Gerbaux, M., Grévy, S., Hukkanen, M., Husson, A., Jaries, A., Jokinen, A., Moore, I.D., Pirinen, P., Romero, J., Stryjczyk, M., Virtanen, V., Zadvornaya, A..  $\beta$ -decay  $q$ -value measurement of  $^{136}\text{Cs}$  and its implications for neutrino studies. *Phys Rev C* 2023;108:045502. URL: <https://link.aps.org/doi/10.1103/PhysRevC.108.045502>. doi:10.1103/PhysRevC.108.045502.
  35. Eronen, T., Hardy, J.C.. High-precision  $Q_{EC}$ -value measurements for superallowed decays. *European Physical Journal A* 2012;48(4):1–8. URL: <http://dx.doi.org/10.1140/epja/i2012-12048-y>. doi:10.1140/epja/i2012-12048-y.
  36. Moore, I.D., Eronen, T., Gorelov, D., Hakala, J., Jokinen, A., Kankainen, A., Kolhin, V.S., Koponen, J., Penttilä, H., Pohjalainen, I., Reponen, M., Rissanen, J., Saastamoinen, A., Rinta-Antila, S., Sonnenschein, V., Äystö, J.. Towards commissioning the new IGISOL-4 facility. *Nuclear Instruments and Methods in Physics Research, Section B: Beam Interactions with Materials and Atoms* 2013;317(PART B):208–213. URL: <http://www.sciencedirect.com/science/article/pii/S0168583X13007143><http://dx.doi.org/10.1016/j.nimb.2013.06.036>. doi:10.1016/j.nimb.2013.06.036.
  37. Kolhin, V.S., Eronen, T., Gorelov, D., Hakala, J., Jokinen, A., Jokiranta, K., Kankainen, A., Koikkalainen, M., Koponen, J., Kulmala, H., Lantz, M., Mattera, A., Moore, I.D., Penttilä, H., Pikkarainen, T., Pohjalainen, I., Reponen, M., Rinta-Antila, S., Rissanen, J., Rodríguez Triguero, C., Rytönen, K., Saastamoinen, A., Solders, A., Sonnenschein, V., Äystö, J.. Recommissioning of JYFLTRAP at the new IGISOL-4 facility. *Nuclear Instruments and Methods in Physics Research, Section B: Beam Interactions with Materials and Atoms* 2013;317(PART B):506–509. URL: <http://www.sciencedirect.com/science/article/pii/S0168583X13008641>. doi:10.1016/j.nimb.2013.07.050.
  38. Karvonen, P., Moore, I.D., Sonoda, T., Kessler, T., Penttilä, H., Peräjärvi, K., Ronkanen, P., Äystö, J.. A sextupole ion beam guide to improve the efficiency and beam quality at IGISOL. *Nuclear Instruments and Methods in Physics Research, Section B: Beam Interactions with Materials and Atoms* 2008;266(21):4794–4807. URL: <http://www.sciencedirect.com/science/article/B6TJN-4T2S8KR-1/2/1d7624cd369335096dcbf1d81a410fea>. doi:10.1016/j.nimb.2008.07.022.
  39. Nieminen, A., Huikari, J., Jokinen, A., Äystö, J., Campbell, P., Cochrane, E.C.. Beam cooler for low-energy radioactive ions. *Nuclear Instruments and Methods in Physics Research, Section A: Accelerators, Spectrometers, Detectors and Associated Equipment* 2001;469(2):244–253. URL: <http://www.sciencedirect.com/science/article/B6TJM-43PGJKX-C/1/93d5587efba5cf8e8571b63228952dab8>. doi:10.1016/S0168-9002(00)00750-6.
  40. Savard, G., Becker, S., Bollen, G., Kluge, H.J., Moore, R.B., Otto, T., Schweikhard, L., Stolzenberg, H., Wiess, U.. A new cooling technique for heavy ions in a Penning trap. *Physics Letters A* 1991;158(5):247–252. URL: [https://doi.org/10.1016/0375-9601\(91\)91008-2](https://doi.org/10.1016/0375-9601(91)91008-2). doi:10.1016/0375-9601(91)91008-2.
  41. Eronen, T., Elomaa, V.V., Hager, U., Hakala, J., Jokinen, A., Kankainen, A., Rahaman, S., Rissanen, J., Weber, C., Äystö, J.. JYFLTRAP: Mass spectrometry and isomerically clean beams. *Acta Physica Polonica B* 2008;39(2):445–455. URL: <https://www.actaphys.uj.edu.pl/R/39/2/445/pdf>.
  42. Nesterenko, D.A., Eronen, T., Ge, Z., Kankainen, A., Vilen, M.. Study of radial motion phase advance during motion excitations in a penning trap and accuracy of jyfltrap mass spectrometer. *Eur Phys J A* 2021;57:302. URL: <https://doi.org/10.1140/epja/s10050-021-00608-3>.
  43. Nesterenko, D.A., Eronen, T., Kankainen, A., Canete, L., Jokinen, A., Moore, I.D., Penttilä, H., Rinta-Antila, S., de Roubin, A., Vilen, M.. Phase-Imaging Ion-Cyclotron-Resonance technique at the JYFLTRAP double Penning trap mass spectrometer. *European Physical Journal A* 2018;54(9):0–13. URL: <https://dx.doi.org/10.1140/epja/i2018-12589-y>. doi:10.1140/epja/i2018-12589-y.

44. Eliseev, S., Blaum, K., Block, M., Dörr, A., Droese, C., Eronen, T., Goncharov, M., Höcker, M., Ketter, J., Ramirez, E.M., Nesterenko, D.A., Novikov, Y.N., Schweikhard, L.. A phase-imaging technique for cyclotron-frequency measurements. *Applied Physics B: Lasers and Optics* 2014;114(1-2):107–128. URL: <http://dx.doi.org/10.1007/s00340-013-5621-0>. doi:10.1007/s00340-013-5621-0.
45. Eliseev, S., Blaum, K., Block, M., Droese, C., Goncharov, M., Minaya Ramirez, E., Nesterenko, D.A., Novikov, Y.N., Schweikhard, L.. Phase-imaging ion-cyclotron-resonance measurements for short-lived nuclides. *Physical Review Letters* 2013;110(8):82501. URL: <https://link.aps.org/doi/10.1103/PhysRevLett.110.082501>. doi:10.1103/PhysRevLett.110.082501.
46. Kramida, A., Yu. Ralchenko, , Reader, J., and NIST ASD Team, . NIST Atomic Spectra Database (ver. 5.8), [Online]. Available: <https://physics.nist.gov/asd> [2021, January 19]. National Institute of Standards and Technology, Gaithersburg, MD.; 2020.
47. Wang, M., Huang, W., Kondev, F., Audi, G., Naimi, S.. The AME 2020 atomic mass evaluation (II). tables, graphs and references\*. *Chinese Physics C* 2021;45(3):030003. URL: <https://doi.org/10.1088/1674-1137/abddaf>. doi:10.1088/1674-1137/abddaf.
48. National nuclear data center. Available at <https://www.nndc.bnl.gov/> (2020/4/7); 2021. URL: <https://www.nndc.bnl.gov/>.
49. Wiedeking, M., Krčíčka, M., Bernstein, L.A., Allmond, J.M., Basunia, M.S., Bleuel, D.L., Harke, J.T., Daub, B.H., Fallon, P., Firestone, R.B., Goldblum, B.L., Hatarik, R., Lake, P.T., Larsen, A.C., Lee, I.Y., Lesher, S.R., Paschalidis, S., Petri, M., Phair, L., Scielzo, N.D., Volya, A..  $\gamma$ -ray decay from neutron-bound and unbound states in  $^{95}\text{Mo}$  and a novel technique for spin determination. *Phys Rev C* 2016;93:024303. URL: <https://link.aps.org/doi/10.1103/PhysRevC.93.024303>. doi:10.1103/PhysRevC.93.024303.
50. Basu, S.K., Mukherjee, G., Sonzogni, A.A.. Nuclear data sheets for  $A = 95$ . *Nuclear Data Sheets* 2010;111(10-11):2555–2737. doi:10.1016/j.nds.2010.10.001.
51. Thompson, A., Lindau, I., Attwood, D., Liu, Y., Gullikson, E., Pianetta, P., Howells, M., Robinson, A., Kim, K., Scofield, J., Kirz, J., Underwood, J., Kortright, J., Wiliams, G., Winick, H.. X-RAY DATA BOOKLET. Berkeley, California: Lawrence Berkeley National Laboratory; 2009.
52. Kellerbauer, A., Blaum, K., Bollen, G., Herfurth, F., Kluge, H.J., Kuckein, M., Sauvan, E., Scheidenberger, C., Schweikhard, L.. From direct to absolute mass measurements: A study of the accuracy of ISOLTRAP. *European Physical Journal D* 2003;22(1):53–64. URL: <http://dx.doi.org/10.1140/epjd/e2002-00222-0>. doi:10.1140/epjd/e2002-00222-0.
53. Roux, C., Blaum, K., Block, M., Droese, C., Eliseev, S., Goncharov, M., Herfurth, F., Ramirez, E.M., Nesterenko, D.A., Novikov, Y.N., Schweikhard, L.. Data analysis of Q-value measurements for double-electron capture with SHIPTRAP. *The European Physical Journal D* 2013;67(7):1–9. URL: <http://dx.doi.org/10.1140/epjd/e2013-40110-x>. doi:10.1140/epjd/e2013-40110-x.
54. Birge, R.T.. The calculation of errors by the method of least squares. *Physical Review* 1932;40(2):207–227. URL: <https://link.aps.org/abstract/PR/v40/p207>. doi:10.1103/PhysRev.40.207.
55. Huang, W., Wang, M., Kondev, F., Audi, G., Naimi, S.. The AME 2020 atomic mass evaluation (I). evaluation of input data, and adjustment procedures\*. *Chinese Physics C* 2021;45(3):030002. URL: <https://doi.org/10.1088/1674-1137/abdd0>. doi:10.1088/1674-1137/abdd0.
56. Langer, L.M., Wortman, D.E.. Radioactive decay of  $\text{nb}^{95}$ . *Phys Rev* 1963;132:324–328. URL: <https://link.aps.org/doi/10.1103/PhysRev.132.324>. doi:10.1103/PhysRev.132.324.
57. Cretzu, T., Hohmuth, K., Schintlmeister, J.. Der zerfall von  $\text{tc}^{95}\text{m}$ . *Nuclear Physics* 1965;70(1):129–140. URL: <https://www.sciencedirect.com/science/article/pii/0029558265902294>. doi:[https://doi.org/10.1016/0029-5582\(65\)90229-4](https://doi.org/10.1016/0029-5582(65)90229-4).
58. N.M.Antoneva, , A.V.Barkov, , A.V.Zolotavin, , P.P.Dmitriev, , S.V.Kamynov, , G.S.Katykhin, , E.T.Kondrat, , N.I.Krasnov, , Y.N.Podkopaev, , V.A.Sergienko, , V.I.Fominykh, . The decay of  $^{95}\text{tc}$ . *IzvAkadNauk* 1974;SSSR:Ser.Fiz. 38, 48.
59. J.A.Pinston, , E.Monnand, , A.Moussa, . Desintegration de  $^{95}\text{ru}$ . *JPhys(Paris)* 1968;29:257.
60. Sevestrean, V.A., Nițescu, O., Ghinescu, S., Stoica, S.. Self-consistent calculations for atomic electron capture. *Phys Rev A* 2023;108:012810. URL: <https://link.aps.org/doi/10.1103/PhysRevA.108.012810>. doi:10.1103/PhysRevA.108.012810.
61. Salvat, F., Fernández-Varea, J.M.. radial: A fortran subroutine package for the solution of the radial schrödinger and dirac wave equations. *Computer Physics Communications* 2019;240:165–177. URL: <https://www.sciencedirect.com/science/article/pii/S0010465519300633>. doi:<https://doi.org/10.1016/j.cpc.2019.02.011>.
62. Hahn, B., Ravenhall, D.G., Hofstadter, R.. High-energy electron scattering and the charge distributions of selected nuclei. *Phys Rev* 1956;101:1131–1142. URL: <https://link.aps.org/doi/10.1103/PhysRev.101.1131>. doi:10.1103/PhysRev.101.1131.
63. CAMPBELL, J., PAPP, T.. Widths of the atomic k-n7 levels. *Atomic Data and Nuclear Data Tables* 2001;77(1):1–56. URL: <https://www.sciencedirect.com/science/article/pii/S0092640X00908489>. doi:<https://doi.org/10.1006/adnd.2000.0848>.
64. Behrens, H., Bühring, W.. Electron Radial Wave Functions and Nuclear Beta-decay (International Series of Monographs on Physics). Oxford: Clarendon press; 1982.
65. Suhonen, J.. From Nucleons to Nucleus. Springer, Gaithersburg MD, 20899; Springer-Verlag Berlin Heidelberg; 2007. URL: <https://www.springer.com/gp/book/9783540488590#aboutBook>. doi:10.1007/978-3-540-48861-3.
66. Honma, M., Otsuka, T., Mizusaki, T., Hjorth-Jensen, M.. Effective interaction for f5pg9-shell nuclei and two-neutrino double beta-decay matrix elements. *Journal of Physics: Conference Series* 2006;49(1):45. URL: <https://dx.doi.org/10.1088/1742-6596/49/1/011>. doi:10.1088/1742-6596/49/1/011.
67. Barea, J., Kotila, J., Iachello, F.. Nuclear matrix elements for double- $\beta$  decay. *Phys Rev C* 2013;87:014315. URL: <https://link.aps.org/doi/10.1103/PhysRevC.87.014315>. doi:10.1103/PhysRevC.87.014315.
68. Suhonen, J.T.. Value of the axial-vector coupling strength in  $\beta$  and  $\beta\beta$  decays: A review. *Frontiers in Physics* 2017;5. URL: <https://www.frontiersin.org/articles/10.3389/fphy.2017.00055>. doi:10.3389/fphy.2017.00055.
69. Mougeot, X.. Improved calculations of electron capture transitions for decay data and radionuclide metrology. *Applied Radiation and Isotopes* 2018;134:225–232. URL: <https://www.sciencedirect.com/science/article/pii/S0969804317304372>. doi:<https://doi.org/10.1016/j.apradiso.2017.07.027>.
70. Hinfurth, B., Hagn, E., Zech, E., Tröger, W., Butz, T.. Measurements of magnetic moments of tc isotopes and the hyperfine field of tc in fe and ni. *Zeitschrift für Physik A Hadrons and Nuclei* 1995;350(4):311–318. doi:10.1007/bf01291188.
71. Proctor, W.G., Yu, F.C.. On the nuclear magnetic moments of several stable isotopes. *Physical Review* 1951;81(1):20–30. doi:10.1103/physrev.81.20.
72. Alzner, A., Bodenstedt, E., Gemünden, G., Herrmann, C., Münnig, H., Reif, H., Rudolph, H.J., Vianden, R., Wrede, U.. Gyromagnetic ratios of the 3/2+ core vibration states of  $^{101}\text{ru}$  and  $^{95}\text{mo}$ . *Zeitschrift für Physik A Atoms and Nuclei* 1984;317(1):107–115. doi:10.1007/bf01420454.
73. Stone, N.. Table of Nuclear Electric Quadrupole Moments. 2021. doi:10.61092/iaea.a6te-dg7q.
74. Brown, B., Rae, W.. The shell-model code NuShellX@MSU. *Nuclear Data Sheets* 2014;120:115–118. URL: <https://doi.org/10.1016/j.nds.2014.07.022>. doi:10.1016/j.nds.2014.07.022.
75. Machleidt, R.. High-precision, charge-dependent bonn nucleon-nucleon potential. *Physical Review C* 2001;63(2):024001. doi:10.1103/physrevc.63.024001.
76. Vaquero, V., Jungclaus, A., Aumann, T., Tscheuschner, J., Litvinova, E.V., Tostevin, J.A., Baba, H., Ahn, D.S., Avigo, R., Boretzky, K., Bracco, A., Caesar, C., Camera, F., Chen, S., Derya, V., Doornenbal, P., Endres, J., Fukuda, N., Garg, U., Giaz, A., Harakeh,

- M.N., Heil, M., Horvat, A., Ieki, K., Imai, N., Inabe, N., Kalantar-Nayestanaki, N., Kobayashi, N., Kondo, Y., Koyama, S., Kubo, T., Martel, I., Matsushita, M., Million, B., Motobayashi, T., Nakamura, T., Nakatsuka, N., Nishimura, M., Nishimura, S., Ota, S., Otsu, H., Ozaki, T., Petri, M., Reifarth, R., Rodríguez-Sánchez, J.L., Rossi, D., Saito, A.T., Sakurai, H., Savran, D., Scheit, H., Schindler, F., Schrock, P., Semmler, D., Shiga, Y., Shikata, M., Shimizu, Y., Simon, H., Stepenbeck, D., Suzuki, H., Sumikama, T., Symochko, D., Syndikus, I., Takeda, H., Takeuchi, S., Taniuchi, R., Togano, Y., Tsubota, J., Wang, H., Wieland, O., Yoneda, K., Zenihiro, J., Zilges, A.. Fragmentation of single-particle strength around the doubly magic nucleus  $^{132}\text{Sn}$  and the position of the  $0f_{5/2}$  proton-hole state in  $^{131}\text{In}$ . *Phys Rev Lett* 2020;124:022501. URL: <https://link.aps.org/doi/10.1103/PhysRevLett.124.022501>. doi:10.1103/PhysRevLett.124.022501.
77. Lisetskiy, A.F., Brown, B.A., Horoi, M., Grawe, H.. New  $t = 1$  effective interactions for the  $f_{5/2} p_{3/2} p_{1/2} g_{9/2}$  model space: Implications for valence-mirror symmetry and seniority isomers. *Phys Rev C* 2004;70:044314. URL: <https://link.aps.org/doi/10.1103/PhysRevC.70.044314>. doi:10.1103/PhysRevC.70.044314.
78. Mach, H., Warburton, E.K., Gill, R.L., Casten, R.F., Becker, J.A., Brown, B.A., Winger, J.A.. Meson-exchange enhancement of the first-forbidden  $^{96}\text{Y}^g(0^-) \rightarrow {}^{96}\text{Zr}^g(0^+)$   $\beta$  transition:  $\beta$  decay of the low-spin isomer of  $^{96}\text{Y}$ . *Phys Rev C* 1990;41:226–242. URL: <https://link.aps.org/doi/10.1103/PhysRevC.41.226>. doi:10.1103/PhysRevC.41.226.
79. Schweiger, C., Braß, M., Debierre, V., Door, M., Dorrer, H., Düllmann, C.E., Enss, C., Filianin, P., Gastaldo, L., Harman, Z., Haverkort, M.W., Herkenhoff, J., Indelicato, P., Keitel, C.H., Kromer, K., Lange, D., Novikov, Y.N., Renisch, D., Rischka, A., Schüssler, R.X., Eliseev, S., Blaum, K.. Penning-trap measurement of the  $q$  value of electron capture in  $^{163}\text{Ho}$  for the determination of the electron neutrino mass. *Nature Physics* 2024;doi:10.1038/s41567-024-02461-9.

### Declaration of competing interest

The authors declare that there are no known competing financial interests or personal relationships that could have appeared to influence the work reported in this paper.

### Acknowledgements

We acknowledge the staff of the Accelerator Laboratory of University of Jyväskylä (JYFL-ACCLAB) for providing stable online beam. We thank the support by the Academy of Finland under the Finnish Centre of Excellence Programme 2012–2017 (Nuclear and Accelerator Based Physics Research at JYFL) and projects No. 306980, 312544, 275389, 284516, 295207, 314733, 315179, 327629, 320062, 354589, 345869 and 354968. The support by the EU Horizon 2020 research and innovation program under grant No. 771036 (ERC CoG MAIDEN) is acknowledged. This project has received funding from the European Union’s Horizon 2020 research and innovation programme under grant agreement No. 861198–LISA–H2020-MSCA-ITN-2019. V.A.S., O.N., S.S., J.S., and J.K. acknowledge support from project PNRR-I8/C9-CF264, Contract No. 760100/23.05.2023 of the Romanian Ministry of Research, Innovation and Digitization. The work leading to this publication was supported by the Deutsche Forschungsgemeinschaft (DFG, German Research Foundation) - AY 155/2-1. The paper was supported by the DAAD Grant No. 57610603.